

PACIFIC GAS AND ELECTRIC COMPANY  
GEOSCIENCES DEPARTMENT  
TECHNICAL REPORT

Report Number: GEO. DCP.P.TR.12.01  
Report Revision: 1  
Report Date: 09/02/2014  
Quality Related: Y  
Page 1 of 53

**REPORT TITLE: DCP.P 3D/2D Seismic-Reflection Investigation of Structures Associated with the Northern Shoreline Seismicity Sublineament of the Point Buchon Region**

**SIGNATORIES**

PREPARED BY:



DATE:

Sept 1, 2014

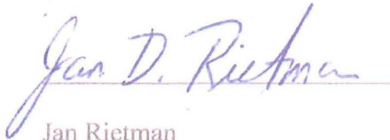
Moss Landing Marine  
Laboratories

H. Gary Greene

Printed Name

Organization

VERIFIED BY:



DATE:

Sept. 2, 2014

Consulting Geophysicist

Jan Rietman

Printed Name

Organization

APPROVED BY:



DATE:

Sept. 10, 2014

Richard Klimczak

Geosciences

Printed Name

Organization

## RECORD OF REVISIONS

Rev. No.	Reason for Revision	Revision Date
0	Initial Report: This work was defined and tracked under SAPN 50427212	12/04/2012
1	<p>This work was defined and tracked under SAPN 50510099</p> <p>Extensive revisions to the text and figures have been made based on comments from the CPUC Independent Peer Review Panel’s review of the original version of this document (Revision 0), stated during a meeting on 29 March 2013, from technical edits, and from undertaking a Nuclear Quality Assurance (NQA) review under PG&amp;E’s Geosciences Quality Assurance (QA) program following Geosciences procedure CF3.GE2. No change bars are presented in the text and figures because of the extensive re-write of the document but major corrections are listed below:</p> <ul style="list-style-type: none"> <li>• Figures were modified to show uninterpreted profiles next to interpreted profiles. The figures addressed are 10, 12, 13, 14, 17, 18, and 19 of Rev. 0 (figures 3-1, 6-1, 6-2, 6-4, 6-7, 6-8, and 6-9 in Rev. 1).</li> <li>• Added a DEM and time slice of bedrock surface with sediment stripped off to show lack of faulting in area (see Figure 6-3).</li> <li>• The objective, purpose, and goals were modified to state that the report is not a source characterization report but a technical report. Specific parts of text addressed include: Page 8 (last paragraph), Page 9 (First paragraph), Page 14 (last paragraph) and Page 15 (last paragraph and “Goals”) of Rev. 0. Note that “seismicity” has been changed to “epicenters alignment”.</li> <li>• Team expertise has been highlighted to indicate that both geophysicists and geologists with much experience were involved in interpretation of data and writing of report (Page 23, last paragraph of Rev. 0).</li> <li>• Criteria for the selection of faults in a fault zone have been clarified.</li> <li>• Editorial corrections have been made on page 28 of Rev. 0 where “or” was changed to “and”.</li> <li>• Clarified how southern part of survey area is disorganized and fragmented (First full paragraph on Page 45 of Rev. 0).</li> <li>• Expanded discussion on relationship of Point Buchon fault to the Shoreline fault as discussed in last paragraph on Page 45 of Rev. 0).</li> <li>• Produced a diagram that shows what the dip of the Point Buchon fault should be at the seismogenic depth (see new Figure 7-1).</li> <li>• Reference in the text to source characterization is clarified by stating that this report is not addressing source characterization.</li> </ul>	09/02/2014

## TABLE OF CONTENTS

	<b>Page</b>
Signatories Page .....	1
Record of Revisions .....	2
Lists of Tables, Figures, Appendices, and Attachments.....	5
Abbreviations and Acronyms .....	8
1.0 INTRODUCTION .....	10
1.1 Purpose .....	11
1.2 Background.....	11
1.2.1 Regional Stratigraphy .....	11
1.2.2 Tectonic Setting.....	12
1.2.3 Key Local Faults .....	14
1.3 Definition of Study Area.....	14
1.4 Goals .....	15
1.5 Intended Use of the Results .....	15
2.0 DATA.....	17
2.1 Data Acquisition .....	17
2.2 Data Processing and Quality Control.....	19
3.0 METHODOLOGY .....	22
3.1 Team-Based Approach .....	22
3.2 Interpretation Tools .....	23
3.3 Interpretation Criteria .....	24
3.3.1 Mapping Horizons (Stratigraphic Beds and Unconformities) .....	24
3.3.2 Mapping Faults .....	24
4.0 ASSUMPTIONS .....	27
5.0 SOFTWARE .....	29
6.0 INTERPRETATION AND ANALYSIS.....	30
6.1 Interpretation.....	30
6.1.1 Interpretability of Data.....	30
6.1.1.1 Poor Interpretability .....	30
6.1.1.2 Good Interpretability.....	32
6.1.2 Stratigraphy .....	32

6.1.3	Structure.....	34
6.2	Analysis .....	35
6.2.1	Hosgri Fault Zone .....	36
6.2.1.1	Northern Part of Study Area .....	36
6.2.1.2	Southern Part of Study Area .....	38
6.2.2	Point Buchon Fault Zone .....	38
6.2.2.1	Main Trace of Point Buchon Fault Zone .....	39
6.2.2.2	East Branch Point Buchon Fault Zone.....	40
6.2.2.3	Western Splays of the Point Buchon Fault Zone .....	41
6.2.3	Structures Coincident with the Northern Shoreline Seismicity Sublineament .....	41
6.2.3.1	Folds.....	41
6.2.3.2	Complex Structural Area .....	42
6.2.3.3	Northern Extent of the Shoreline Seismicity Trend at the Hosgri Fault Zone .....	43
7.0	CONCLUSIONS .....	44
7.1	The Hosgri Fault Zone.....	44
7.2	The Point Buchon Fault Zone.....	45
7.3	Folding .....	45
7.4	Northern Shoreline Seismicity Sublineament.....	46
7.5	Strike-Slip Tectonic Models .....	47
8.0	LIMITATIONS .....	48
9.0	IMPACT EVALUATION .....	49
10.0	REFERENCES .....	50

## LISTS OF TABLES, FIGURES, PLATES, APPENDICES, AND ATTACHMENTS

### Tables

- Table 2-1 Fugro 2010–2011 3D Seismic Acquisition Parameters
- Table 3-1 Numbering System and Colors Used to Distinguish Fault Types and Association with Fault Zones and Groups (Trends) on the High-Resolution 3D/2D Seismic-Reflection Survey Area Offshore of DCP.P

### Figures

- Figure 1-1 Regional Tectonic Setting with Faults and Structural Domains (Modified from PG&E, 1988)
- Figure 1-2 Structural Blocks and Faults in the DCP.P Area (Modified from PG&E, 1988)
- Figure 1-3 Frequency Spectrum from 3D/2D Seismic-Reflection Data Set Showing Dominant (Fundamental) Frequency of 200–225 Hz and Calculation Using 1,600–1,650 m/s to Determine Vertical Resolution (2.00–2.06 and 1.78–1.83 m)
- Figure 2-1 Streamer Layout (Layback Diagram) for Seismic Source and Receivers Used in the Collection of 3D/2D Data from the M/V *Michael Uhl*
- Figure 2-2 Trackline Map of 2D Seismic-Reflection Lines and Boundary of 3D Survey Area
- Figure 2-3 Schematic Diagram of Streamer Array Showing Navigation Positioning Accuracy During 3D/2D Seismic-Reflection Survey
- Figure 2-4 Schematic Diagram Illustrating Skewed Geometry of Streamer Array During Times of Adverse Weather Conditions Resulting in Irregular Coverage
- Figure 2-5 Example of “Bubble Pulse” Recorded During 3D/2D Seismic-Reflection Survey Showing ~5 ms (~4 m) Thick Shallow Subsurface Section Not Resolvable due to Masking of Legitimate Reflectors by Pulse Width
- Figure 2-6 Flow Chart Showing Procedures and Steps Undertaken in the Processing of the 3D Data

- Figure 3-1 Examples of Data Quality (Interpretability) Shown in (a, b) 3D Seismic-Reflection Profiles Line 12120 and on (c) Amplitude Time Slice at 150 ms (TWTT)
- Figure 4-1 MBES Bathymetry Overlain on 3D Amplitude Time Slice at 138 ms (TWTT) Showing a Good Correlation Between the Two Data Sets
- Figure 6-1 Example of a Wave-Cut Platform and Shoreline Angles Illustrated in 3D Seismic-Reflection Profile 13340 and Showing Bedding Artifacts
- Figure 6-2 Illustrations of Mobile Sand Sheets Shown in (a, b) 3D Seismic-Reflection Profiles 12120 and on (c) MBES Shaded Relief Bathymetry Map
- Figure 6-3 DEM of Bedrock Surface with Sediment Removed in the Point Buchon Study Area
- Figure 6-4 Vertical and Horizontal Geometry of Hosgri Fault Zone Strands in (a, b) 3D Seismic-Reflection Profiles 11180 and on (c) MBES Bathymetry Map Within Northern Part of Survey Area
- Figure 6-5 Amplitude Time-Slice Maps at 95 ms (TWTT) in Southern Part of 3D Study Area Showing (a) Uninterpreted and (b) Interpreted Strands of the Point Buchon Fault Zone
- Figure 6-6 Fault Strands Associated with Fault Intersection of Point Buchon Fault Zone Shown in (a) Uninterpreted and (b) Interpreted Similarity Time Slices at 74 ms (TWTT)
- Figure 6-7 Graben at Northern End of Point Buchon Fault Zone Shown on (a, b) 2D Seismic-Reflection Profiles 1120 and (c) MBES Bathymetry
- Figure 6-8 Structure Associated with Northern Part of Point Buchon Fault Zone Shown in (a, b) 3D Seismic-Reflection Profiles 11820 and (c) Amplitude Time Slice at 150 ms (TWTT)
- Figure 6-9 Principal Structural Elements in Northern Part of Study Area Showing Faults and Folds in (a, b) 2D Seismic-Reflection Profiles 1399 and on (c) Amplitude Time-Slice Map at 150 ms (TWTT)
- Figure 6-10 Seismicity and Focal Mechanisms in the Study Area
- Figure 7-1 Seismicity in Relation to Depth of 3D/2D Seismic-Reflection Penetration

### **Foldout Figures**

- Foldout A Comparison of Amplitude and Similarity Time Slices at 150 ms Showing Uninterpreted Data (a and b) and Interpreted Maps (c and d)
- Foldout B Marker Horizons Identified in (a) User-Selected 3D Strike Line and (b) Mapped on Amplitude Time Slice at 150 ms (TWTT)

- Foldout C Graben Associated with Hosgri Fault Zone: (a) 2D Seismic-Reflection Profile 1039 Showing Fault Boundaries and Sediment Fill and (b) Map View Showing Faults, Graben, and MBES Bathymetry
- Foldout D Relationship of the Hosgri and Point Buchon Fault Zones in Northern Part of Survey Area: (a) Uninterpreted and (b) Interpreted 3D Profile 11200; (c) Uninterpreted and (d) Interpreted Amplitude Time Slice at 150 ms (TWTT)

## **Plates**

- Plate 1 Geology of Interpreted Offshore Structures from the 2011 Shoreline Fault Zone Report (PG&E, 2011b)
- Plate 2 Structure Map Based on Low-Energy 3D/2D Seismic-Reflection Data
- Plate 3 Comparison of Interpreted Offshore Structures: a Shoreline Fault Zone Report (PG&E, 2011b) and b This Study

## **Appendices**

- Appendix A Qualification of Point Buchon 3D & 2D Seismic-Reflection Profiling Survey Data (October 2010 to February 2011)

## **Attachments**

- Attachment 1 Report Verification Summary

## ABBREVIATIONS AND ACRONYMS

2D	two-dimensional
3D	three-dimensional
CSUMB	California State University Monterey Bay
CCCSIP	Central Coastal California Seismic Imaging Project
CDP	common depth point
CEG	Civil Engineering Geologist (California)
DCPP	Diablo Canyon Power Plant
DGPS	differential global positioning system
GPS	global positioning system
HFZ	Hosgri Fault Zone
HESS	high-energy seismic survey
Hz	hertz
IHO	International Hydrographic Office
ITR	Independent Technical Reviewer
kJ	kilojoules
km	kilometers
km <sup>2</sup>	square kilometers
LESS	low-energy seismic survey
LTSP	Long Term Seismic Program
m	meters
Ma	million years ago ( <i>or</i> million years old)
MBES	multibeam echosounder
MLLW	mean-lower-low-water
mm/yr	millimeters per year
ms	milliseconds
m/s	meters per second
MSL	mean sea level
NMO	normal moveout
NOAA	National Oceanic and Atmospheric Administration
NQA	Nuclear Quality Assurance



NRC	U.S. Nuclear Regulatory Commission
PG&E	Pacific Gas and Electric Company
QA	Quality Assurance
QC	Quality Control
RSA	Rock Solid Attributes
s	seconds
SAPN	SAP [software] notification
SMT	Seismic Micro-Technology
SPW	Seismic Processing Workshop
SRME	surface-related multiple elimination
SSC	seismic source characterization
SSHAC	Senior Seismic Hazard Advisory Committee
TI	Technical Integration
TT	tuning thickness
TWTT	two-way travel time
USGS	U.S. Geological Survey
UTM	Universal Transverse Mercator
VR	vertical resolution
WGS	World Geodetic System

## 1.0 INTRODUCTION

Recent studies of seismicity in the vicinity of Pacific Gas and Electric Company's (PG&E) Diablo Canyon Power Plant (DCPP) show a microseismicity (small earthquakes) alignment subparallel to, and 1 kilometer (km) west of, the coastline, suggesting the possible presence of a previously unidentified fault approximately 1 km offshore of the DCPP (PG&E, 2008; Hardebeck, 2010). This previously unidentified fault was named the Shoreline fault zone (PG&E, 2008). An extensive investigation was conducted by PG&E in 2009 and 2010 to better constrain the four main parameters of the Shoreline fault zone that are required for seismic source characterization and the assessment of seismic hazard. These parameters consist of geometry (i.e., fault length, fault dip, downdip width), segmentation, distance from the DCPP, and slip rate. The investigation involved the acquisition, processing, and interpretation of new geologic, seismological, bathymetric, and geophysical data, including seismic-reflection profiles obtained from the U.S. Geological Survey (USGS) in 2008 and 2009 (PG&E, 2011a, 2011b).

As described in two reports by PG&E (2011a, 2011b), the Shoreline fault zone consists of three segments (north, central, and south) segments with distinct geologic, morphologic and geophysical characteristics. Based on data available at the time of the study, the north segment was defined primarily by hypocenter alignments of small earthquakes, as there was no clear geologic or geophysical evidence for the presence of a fault. The earthquake alignment trends northwest and toward the Hosgri Fault Zone (herein referred to as the "HFZ"). In contrast, characteristics of the central and south segments were based on a combination of geophysical anomalies, seafloor geology, and geomorphologic characteristics identified in multibeam echosounder (MBES) bathymetry data in addition to earthquake locations.

To determine the shallow geologic conditions along the proposed north segment of the Shoreline fault, PG&E commissioned low-energy, high-resolution three-dimensional (3D) and two-dimensional (2D) seismic-reflection profiling surveys, called here "low-energy seismic surveys" (LESS), offshore of Point Buchon. The surveys were undertaken in late 2010 and early 2011 and were designed to cover the area where the proposed north segment of the Shoreline fault zone (PG&E, 2011b) was inferred to trend into the HFZ (Plate 1). These surveys significantly filled data voids between the previous seismic-reflection data and provided data for refining interpretations. The low-energy sound source restricted penetration to the shallow subsurface, but allowed for high-resolution acoustic imaging that facilitated structural interpretation within a small area offshore of Point Buchon.

Although the acquisition, processing, and presentation of the 2010–2011 data initially analyzed in Revision 0 of this report were not performed under a Nuclear Quality Assurance (NQA) program that meets the requirements of 10 CFR 50, Appendix B, "Quality Assurance Criteria for Nuclear Power Plants and Fuel Reprocessing Plants," this technical report, was written, reviewed, and approved under the PG&E Geosciences Quality Assurance (QA) program following Geosciences procedure CF3.GE2, Quality Related Technical Reports. The Quality Verification Plan for this report is tracked in SAPN 50427212. Fugro Consultants, Inc., validated the 3D and 2D data processing

software and the software used to interpret the data, and qualified the processed data for use in safety-related applications (see Section 5.0). To ensure that the input data presented in this technical report are qualified for use in safety-related applications, corroboration of the data inputs was performed by Independent Technical Reviewer (ITR) Dr. Jan D. Rietman (in accordance with NQA-1-2008, Part 3, Sub-paragraph 3.3, Appendix 3.1, “Guidance for Qualification of Existing Data”). Details of the software validations and Dr. Rietman’s corroboration are documented in his Verification Summary (Attachment 1) and in Appendix A.

The limitations on the use of the results and conclusions presented in this report are addressed in Section 8.

## **1.1 Purpose**

The purpose of this technical report is to present a revised document (GEO.DCPP.TR.12.01.R1) of the geologic and geophysical interpretations of the offshore low-energy, high-resolution 3D and 2D seismic-reflection data (referred to here as the 3D/2D data set) collected in late 2010 and early 2011 that was originally presented in GEO.DCPP.TR.12.01.R0. The reason for this revision is to address comments and questions provided by the Independent Peer Review Panel (IPRP) at a meeting in San Luis Obispo on 29 March 2013, to clarify text and figures based on a technical edit, and to refine based on the qualification of the report under NQA. Because of the extensive revisions made to this document no change bars are shown.

The results of this study will be integrated with other studies in the Central Coastal California Seismic Imaging Project (CCCSIP) Report (PG&E, 2014) to update the seismic hazard assessment for the DCPP. Faults that contribute most to seismic hazard at the DCPP include the Hosgri, Los Osos, Shoreline, and San Luis Bay fault zones (PG&E, 2011a, 2011b). This report is not a source characterization analysis but provides information that may be used to better characterize the Shoreline and, to a lesser extent, HFZ, thereby reducing uncertainties in the source parameters (i.e., fault length, segmentation and location with respect to DCPP).

## **1.2 Background**

This section presents a brief summary of the geologic and tectonic setting of the study area to provide a contextual framework for the observations and interpretations made from the newly acquired 3D/2D data set. The study area consists of two (3D and 2D) overlapping survey blocks and is located offshore along the coastal margin of the Irish Hills, a west-northwest-trending ridge within the south-central part of the California Coast Ranges, near the city of San Luis Obispo (Plate 1).

### **1.2.1 Regional Stratigraphy**

As part of the work performed to characterize the Shoreline fault zone, PG&E constructed a geologic map of the onshore and offshore areas along the coastline from Morro Bay south to Pismo Beach and west to the offshore shelf break (approximately coincident with the HFZ; PG&E, 2011b). The onshore part of this map is based on a

compilation of existing geologic maps, which were updated to incorporate new detailed geologic mapping of bedrock exposed in the modern sea cliffs. The offshore part of this map was constructed from the interpretation of seafloor relief and texture exhibited in the MBES imagery and correlation of these seafloor features with drop cores and diver-collected bedrock samples that were obtained in early 2010. The part of this geologic map that covers the 3D/2D study area is reproduced on Plate 1.

Basement rocks exposed in the Central California coastal region generally consist of Jurassic to Cretaceous Franciscan Complex rocks (primarily mélangé, metavolcanics, ophiolite, and serpentine), faulted against Cretaceous marine arkosic to lithic sandstone. Along the coastline, the basement rocks are unconformably overlain by the early to middle Miocene Obispo Formation, which consists of tuffaceous marine sandstone, diabase, and resistant zeolitized tuff. Although they are not present along the coastline (on the south limb of the Pismo syncline, the axis of which generally follows the crest of the Irish Hills), the Oligocene Rincon and Vaqueros formations are known to unconformably overlie pre-Tertiary rocks on the north limb of the Pismo syncline in Los Osos Valley. However, the resolution of available geophysical data does not allow for confident differentiation of the Rincon and Vaqueros formations from the basal part of the Obispo Formation. Therefore, in this study, Rincon and Vaqueros strata are considered part of the basal Obispo Formation. The Obispo Formation is unconformably overlain by marine chert, siltstone, diatomite, and porcelaneous shale of the Miocene Monterey Formation (see Legend, Plate 1). The Monterey Formation is well exposed in sea cliffs along an approximately 5.5 km long stretch of coastline near Point Buchon. The late Miocene to Pliocene Pismo Formation unconformably overlies the Monterey Formation and includes, from oldest to youngest, the Miguelito, Edna, Gragg, Belleview, and Squire members. Onshore adjacent to the study area claystone and siltstone of the Miguelito Member are exposed in sea cliffs between Point Buchon and an area near where the Los Osos fault projects into Quaternary aeolian deposits near Morro Bay.

Geologic mapping reported in the Shoreline Fault Zone Report (PG&E, 2011b) shows that the seafloor is underlain by Quaternary marine sediment in a large part of the study area (Plate 1). Where this sediment is absent, most of the seafloor is composed of Tertiary strata exposed in stratigraphic sequences from south to north, including Obispo Formation, Monterey Formation, and the Miguelito Member of the Pismo Formation. Basement rock of the Franciscan Complex and Cretaceous sandstone locally underlie the southernmost part of the study area.

### **1.2.2 Tectonic Setting**

The central coast of California is characterized by transpressional deformation between the San Andreas Fault Zone to the east and the San Gregorio–San Simeon–Hosgri fault system of near-coastal faults to the west (Figure 1-1). Transpressional deformation in the region is likely driven by three distinct but interacting processes (Lettis et al., 2004):

1. Northward left transfer of slip from the San Andreas Fault Zone to the Rinconada and West Huasna faults to the Hosgri–San Simeon fault zone.

2. Clockwise rotation of the western Transverse Ranges domain (transrotational deformation of Luyendyk (1991) and Dickinson (2004a, 2004b), which imparts north-directed strain into the region.
3. An unknown amount of possible plate-normal convergence across the region.

This transform regime initiated approximately 30 million years ago (Ma), when the transform process between the Pacific and North American Plates introduced an episode of strike-slip tectonics, or wrench tectonics (Wilcox et al., 1973), that prevails today (Atwater, 1970). An important aspect of strike-slip tectonic settings is the development of “restraining” and “releasing” bends of a strike-slip fault system (Mann, 2007). The resulting “wrench” deformation is reflected in modern topography and bathymetry of en echelon linear to lens-shaped ridges and rhomboid basins (Howell et al., 1980). In such a dynamic tectonic regime, wrench faults express compression and tension through restraining and releasing bends that accompany lateral displacement. This type of deformation has been well illustrated in clay model experiments (e.g., Cloos, 1955; Tchalenko, 1970; Wilcox et al., 1973; Mitra and Paul, 2011) that produced characteristic patterns of drag folds and secondary faults along strike-slip fault zones. Folds form at oblique angles to the strike-slip fault in an en echelon pattern, though if transpression is dominant, the folds are rotated so that they nearly parallel the fault (Harland, 1971). En echelon folds in plastic cover rocks are therefore important indicators of strike-slip faults in more rigid basement rocks at depth (Reading, 1980).

In an en echelon strike-slip fault system, left-stepping right-lateral strike-slip faults produce a zone of compression (transpression) resulting from a restraining bend and uplift between two en echelon faults. By contrast, right-stepping right-lateral strike-slip faults produce a zone of tension (transtension) resulting from a releasing bend and depression between two en echelon faults (Rodgers, 1980). Transtension then forms pull-apart (graben-like) basins, half grabens, or depressions (Buchfiel and Stewart, 1966; Crowell, 1974).

Transpressional deformation has produced several distinct but interacting crustal domains and tectonic structures (Figure 1-1; PG&E, 1988). The study area lies within the western margin of the Los Osos domain, a triangular-shaped structural terrain consisting of northwest-striking reverse, oblique, and strike-slip faults that border uplifted blocks and subsiding basins (valleys). Locally, these include the Santa Maria Valley, San Luis–Pismo, and Los Osos structural blocks, from south to north, respectively (Figure 1-1). The study area is also located in the western offshore part of the San Luis–Pismo structural block. This structural block is bounded to the north by the 50 km long Los Osos fault zone, and to the south by the San Luis Bay, Pecho, Los Berros, Oceano, and Wilmar Avenue faults of the Southwestern Boundary zone (Figures 1-1 and 1-2). The Irish Hills, uplifted ridges and gullies that express the structural core of the San Luis–Pismo block (Figure 1-2). Late Quaternary uplift of the San Luis–Pismo block (Figure 1-2) has been recorded at rates of approximately 0.2 millimeters per year (mm/yr) in the northwest and approximately 0.1 mm/yr in the southeast from a sequence of marine terraces along the western and southern margin of the San Luis Range (Hanson et al., 1994).

### **1.2.3 Key Local Faults**

Faults that contribute most to seismic hazard at the DCP.P include the Hosgri, Los Osos, Shoreline, and San Luis Bay fault zones (PG&E, 2011a, 2011b). This report provides information that may be used to better characterize the Shoreline fault zone and, to a lesser extent, HFZ, thereby reducing uncertainties in the source parameters (i.e., fault length, segmentation and location with respect to DCP.P).

The HFZ trends northwest-southeast for 110 km from north of Point Estero, just north of Estero Bay, to a location approximately 5 km northwest of Point Arguello (Willingham et al., 2013; Figure 1-1). It is considered the southernmost part of the larger 410 km long San Gregorio-San Simeon-Hosgri fault system (Hanson et al., 2004; Dickinson et al., 2005). The Hosgri and San Simeon fault zones accommodate 1 to 3 mm/yr of right slip along steeply dipping to vertical transpressional faults (Hanson et al., 2004). Within the longer connected fault zone, the slip rate increases to the north, accommodating 6 to 8 mm/yr of slip on the San Gregorio fault zone in the Monterey Bay area and northward (Hanson et al., 2004). In the vicinity of the DCP.P, the HFZ is up to 2.5 km wide and composed of multiple fault traces.

As characterized by PG&E (2011b), the Shoreline fault zone is a vertical right-slip fault with an estimated slip rate ranging approximately 0.05–1 mm/yr, with a preferred (best estimated) range of between approximately 0.1 to 0.6 mm/yr. This fault zone has been divided into north, central, and south segments based on changes in the geologic and geophysical expression of faulting at the surface and in the shallow subsurface (PG&E, 2011b). The south and central segments of the Shoreline fault zone are associated with geophysical anomalies and have clear expression in the seafloor geology and geomorphology interpreted from MBES bathymetry data (Plate 1). In contrast, no clear geologic or geophysical expression of the north segment of the Shoreline fault zone was identified in the available data (PG&E, 2011a, 2011b). Earthquakes that defined the northern seismicity lineament, therefore, were not clearly associated with any identified structure. As a result, seismic source models for the Shoreline fault zone included significant uncertainties regarding the extent and location of its north segment.

## **1.3 Definition of Study Area**

The study area is bounded by the limits of the two survey blocks (the 3D and the 2D survey blocks), located offshore and directly northwest of the DCP.P, as shown on Figure 1-2 and Plate 1. The 3D survey covers a T-shaped area within the 2D area, and the 2D survey covers a larger rectangular area. The 3D survey block is 18 square kilometers (km<sup>2</sup>) and is located entirely within the larger 2D survey area (Figure 1-2; Plate 1). The 2D survey consists of 113 lines spaced approximately 100 meters (m) apart, covering an area of 46.5 km<sup>2</sup> (Figure 1-3; Fugro Consultants, 2012a). An additional 1 km<sup>2</sup> square 3D survey block is located to the south of the larger 3D survey block (Plate 1). This smaller survey block was not connected to the larger northern block because of adverse weather conditions and time constraints.

The 3D/2D survey blocks cover the northern section of the Shoreline seismicity sublineament as defined by PG&E (2011b), as well as adjacent parts of the HFZ and the

herein-named “Point Buchon fault zone” (parts of which were called the “N40°W fault” zone in PG&E, 2011b). The widest part (the cross of the T) of the 3D survey covers a part of the HFZ into which the north segment of the Shoreline fault zone was inferred to trend (PG&E, 2011b). The 2D data covers areas in the northern, western, and southern parts of the study area where traces of the HFZ have previously been mapped, and the area between the Hosgri and Shoreline fault zones (Figure 1-2; PG&E, 1988, 2011b).

## 1.4 Goals

The goals of this study were to evaluate the following conditions:

- The character of the 3D/2D data, including the “interpretability,” depth of penetration, and resolution of the data.
- The seismic stratigraphy imaged in the data, including the general extent of stratigraphic units, and potential correlation of mapped horizons with mapped geologic features or units.
- The locations and patterns of faulting, the nature of the faulting, fault strike, dip, vertical separation, evidence for dip-/strike-slip, identification of possible piercing points, and large offset faults versus minor faults (i.e., small offset faults) where the geology is resolvable from the available data.
- The patterns of fold deformation in the data set. This includes trends of folds parallel or oblique to faults, and continuity of folds.
- The nature and complexity of the HFZ within the study area.
- The nature of the Point Buchon fault zone and its relationship with the HFZ (to the north) and the north and central segments of the Shoreline fault zone.
- The nature of the faulting/folding coincident with the northern seismicity sublineament.
- The nature of the intersection of the Shoreline fault zone with the HFZ.
- The nature of geology in areas adjacent to, and between, the Hosgri, Point Buchon, and Shoreline fault zones.
- How the results of this study compare to the previous interpretation of the location and character of the north segment of the Shoreline and Hosgri fault zones (PG&E, 2011a, 2011b).

## 1.5 Intended Use of the Results

The interpretations of the 3D/2D data will be used by PG&E in its ongoing efforts to characterize seismic hazards at the DCP.P. The results of this technical report will be further evaluated and integrated with interpretations of other data sets, including seismicity, previous seismic-reflection surveys, potential field (gravity and magnetic) surveys, and geologic and geomorphic mapping. The data inputs and the final report will

be provided to the DCP Senior Seismic Hazard Advisory Committee (SSHAC) Seismic Source Characterization Technical Integration (SSC TI) team.



## 2.0 DATA

Offshore low-energy, high-resolution 3D and 2D seismic-reflection profile data collected in late 2010 and early 2011 were interpreted for this report. Fugro Consultants, Inc. collected these data specifically for PG&E's use in evaluating the Shoreline fault zone and other faults within the offshore area of the DCP.P. Data collection and processing are described in the following reports:

- Fugro Consultants, Inc. (2012a, 2012b, 2012c, 2012d)
- Fugro Seismic Imaging, Inc. (2012)

The Fugro reports and data, including the 3D and 2D data SEG-Y files, reside in the PG&E Geosciences offices in San Francisco, California.

### 2.1 Data Acquisition

Data were acquired offshore of Point Buchon by Fugro Consultants from 24 November 2010 to 5 February 2011 using standard industry procedures with a low-energy sound source (Table 2-1). Low-energy (1.5 kilojoules [kJ]), high-resolution (100–700 Hertz [Hz] frequency range with a 200–225 Hz fundamental frequency; see Figure 1-3) seismic-reflection profiles were collected using a triple-plate boomer as the acoustic source and four parallel hydrophone streamers for receiving acoustical energy (Figure 2-1). The boomer plates were towed in a sled with the source 0.3 m beneath the sea surface (see Fugro Consultants, Inc., 2012a). A trackline map is presented on Figure 2-2.

The hydrophone streamers were configured and deployed to optimize data collection. Four parallel, 16-channel, 50 m long liquid-filled Geometrics GeoEel™ streamers, with GeoEel hydrophones were grouped at intervals of 3.125 m (42.5 m to first group from head of cable with center group at 25 m from head), and towed at a depth of 2 m ± 0.5 m (see Fugro Consultants, Inc., 2012a; Fugro Seismic Imaging, Inc., 2012). The 3D hydrophone array was configured to have a 6.25 m lateral offset between streamers, providing a subsurface swath width of 18.75 m (Table 2-1). A total of 64 channels of data were acquired with this configuration.

The seismic source (a triple-plate boomer AP3000 manufactured by Subsea Systems, Inc., of Ventura, California, capable of delivering 0.5 kJ of energy/plate) was centered anterior to the hydrophone geometry. Precision horizontal positioning of the receivers and source array was accomplished by placing global positioning system (GPS) units, which used a wide-area differential global positioning system (DGPS), at the head of each hydrophone streamer and the boomer sled (Figure 2-1). The accuracy of positioning varied throughout the streamer array. Data received at the head of the streamer array were collected at a positioning accuracy of approximately 1 m, whereas data received near the tails of the streamers were collected at a positioning accuracy of approximately 3 m (Figure 2-3).

**Table 2-1. Fugro 2010–2011 3D Seismic Acquisition Parameters**

Number of streamers	4
Streamer length	50 m
Channels per streamer	16
Group interval	3.125 m
Streamer type	Geometrics GeoEel Solid Digital
3D swath width	18.75
Bin size	1.563 m x 3.125 m
Nominal subsurface fold	8
Sample rate	0.50 ms
Record length	1.00 s
Recording format	SEG-D
Source type	AP3000 Boomer
Number of plates	3 (2 active)
Power per boomer plate	500 joules
Frequency spectrum	100–700 Hz
Shot interval	3.125 m

The seismic source was fired at 3.125 m intervals with 16 channels per streamer providing for 8-fold acquisition geometry (Fugro Consultants, Inc., 2012a, 2012b). Calculations for fold are as follows:

$$\begin{aligned} \text{Fold} &= (1/2) * (\text{Number of Channels}) * (\text{Channel Interval} / \text{Shot interval}) \\ \text{Fold} &= (1/2) * (16) * (3.125\text{m} / 3.125\text{m}) \\ \text{Fold} &= (1/2) * (16) * (1) \\ \text{Fold} &= 8 \end{aligned}$$

The returning signals and positioning data were digitally transmitted to the recording equipment onboard the M/V *Michael Uhl*. Line spacing was 12.5 m for 3D data acquisition (see Fugro Consultants, 2012a). However, winds, waves, and currents sometimes resulted in uneven streamer separations that prevented the intended coverage (Figure 2-4).

Vertical resolution of the 3D/2D data is estimated to be 1.8–2 m based on a dominant (fundamental) frequency of approximately 200–225 Hz at an assumed velocity of approximately 1,600–1,650 meters per second (m/s; Figure 1-3). Vertical resolution is calculated as follows:

$$VR = TT = 0.25\lambda \text{ (of dominant frequency)}$$

where *VR* is the vertical resolution, *TT* is the tuning thickness, and  $\lambda$  is the wavelength.

Vertical resolution of the collected seismic-reflection data is dependent upon the frequency of the seismic source. The seismic vertical resolution is the minimum (or tuning) thickness of a bed that can be distinguished. The tuning thickness is a bed that is  $0.25\lambda$  in thickness from which reflectors from its upper and lower surfaces interfere. The interference is constructive when the contrasts of the two interfaces are of opposite polarity, often resulting in an exceptionally strong reflection (Sheriff and Geldart, 1995).

Infilling of seismic data gaps was undertaken during January and February of 2011 (Figure 2-4). The 2D data were collected at 100 m spacing in contrast to the 12.5 m line spacing used for the 3D data (see Fugro Consultants, 2012b). Nominal fold was 8, with a sample rate of 0.5 millisecond (ms) and a record length of 1 second (s) for 3D and 2D data. The bin nominal size was  $\sim 1.563$  m in the inline direction and  $\sim 3.125$  m in the crossline direction. A total of 2,019.47 km of 3D and 2D data were collected. The 3D swath mapping (4 streamer width) provided a full-fold area, or cube (referred to as a volume in the industry), of  $17.51 \text{ km}^2$ , which is divided into a large  $16.51 \text{ km}^2$  rectangular block and a small  $1.0 \text{ km}^2$  square block. A total of 113 2D lines were collected (Fugro Consultants, 2012b). Survey deliverables to PG&E that are used in this report are based on World Geodetic System 84 (WGS 84) Universal Transverse Mercator (UTM) Zone 10 (N) meter grid coordinates (see Fugro Consultants, 2012a).

## 2.2 Data Processing and Quality Control

The 2D and 3D data were processed in a similar manner by two organizations. Fugro Consultants, Inc., in Ventura, California, processed the 2D data (Fugro Consultants, 2012b); Fugro Seismic Imaging, Inc., in Houston, Texas, processed the 3D data (Fugro Seismic Imaging, Inc., 2012). All data processing was performed following industry standards (industry standards refer to those standards and procedures of data collection and processing used by petroleum and geophysical companies to assure continuous high quality and consistency in their data acquisition methods) practices for data collection and processing (Fugro Consultants, Inc., 2012a, 2012b) and followed procedures described in the *Handbook of Offshore Surveying* (Lekkerkerk et al., 2006). For every processing stage, the output data and log files were checked for accuracy. Quality control checks were recorded in the project files. The data were processed using Fugro Seismic Imaging's proprietary seismic processing software in UNISEIS™.

Stacks and gathers were created and reviewed for every survey line at each stage of data processing steps. The 3D volume time slices were created and viewed at the following processing milestones: surface-related multiple elimination (SRME) volume, signature deconvolution volume, crossline statics solution, pre-stacked time migration, final filtered, and scaled volume. Velocities were checked in Fugro Seismic Imaging's proprietary analysis software package UNISEIS using an isovelocity viewer and display of normal moveout (NMO) corrected common-depth-point (CDP) gathers. Time slices of the first pass velocity volume and migration velocity volume also were created and viewed. These data are displayed in a 3D volume, or cube, that can be used in a similar manner as a medical computerized tomography (CT) scan to view internal structures and stratigraphy. The data can be viewed in cross-sectional vertical profiles or in horizontal time slices, selected in any direction (often referred to as "arbitrary cross section"), and

are useful for developing maps and measuring true strikes and dips of features. This 3D processing technique provides substantially more information than can be obtained from conventional 2D seismic-reflection profile interpretations and removes considerable uncertainty from the resulting interpretations and analyses.

Velocity analysis was also performed with Fugro Seismic Imaging's proprietary analysis software package in UNISEIS (see Fugro Seismic Imaging, 2012). For this report, depth is reported in two-way travel time (TWTT) in seconds on seismic-reflection profiles and milliseconds in 3D volume time slices, with sea surface being zero; however, a tidal range from +2.1 m to -0.5 m occurred during the surveys, which was determined by the tidal cycles recorded by the National Oceanic and Atmospheric Administration (NOAA) at Port San Luis. Tidal fluctuations were addressed by statistical corrections for statics (variations in tidal elevation, swell, seismic source depth, and streamer depth) during processing of the 2010–2011 3D data collected west of Point Buchon (Figure 1-1); the vertical datum was mean sea level (MSL).

A swell/static filter was applied to get the best possible match of the data bins, but not corrected to a vertical datum such as mean-lower-low-water (MLLW). Depth estimates are based on an assumed shallow subsurface sediment velocity of 1,600 m/s (Fugro Consultants, 2012b).

The seismic stratigraphy immediately beneath the seafloor is masked by the “bubble pulse,” the train of seismic energy produced by the sound source and exhibited in seismic-reflection profiles as a series of closely spaced artifact reflections. Although deconvolution processing was applied, bubble pulse masking prevents complete resolution of weak, legitimate reflections parallel to the seafloor for approximately 5 ms (~4 m at 1,600 m/s) beneath the seafloor reflection (Figure 2-5).

Processing of the 3D seismic-reflection data was a multi-step process, with a quality control assessment made at the end of each step (Figure 2-6). Parameter (e.g., gain, signal-to-noise ratio) testing was initially applied to the data followed by navigation merge and quality control (QC) assessment, initial noise elimination, QC of near-trace gathers, application of low-cut filter, and gain recovery (Figure 2-6). The data were then sorted to CDP and a brute stack for each streamer was produced using a water-dependent brute velocity function. Static corrections were then made to reduce jitter in the data that resulted from a lack of control mechanisms (“birds”) on the streamer to regulate depth and orientation. Noise due to swell, boomer misfires, and other sources was attenuated from the data using a time-frequency denoise algorithm. The SRME algorithm, which included the bubble pulse train to reduce repeated surface reflectors, was utilized, and velocity analysis was performed on a 125 m (inline direction) by 250 m (crossline direction) grid.

The binned multiple reflections within SRME were stacked and a dip model was constructed using a similarity-based dip analysis with Fugro Seismic Imaging's interpolator (see Fugro Seismic Imaging, Inc., 2012). Another dip model was then created using a full stack of the data. Migration velocity analysis and signature deconvolution were conducted using a statistical deconvolution approach, which involved the design of a wavelet-shaping operator for each individual shot record. Lines were migrated post-

stack 2D to be used as input into the crossline solution. Offset plane regularization and interpolation and 3D pre-stack Kirchhoff time migration were subsequently performed. The final, nominal 8-fold binned gathers were output from the 3D migration as NMO and the binned gathers were stacked. Unwanted noise outside of the frequency range of the desired reflection data was attenuated by the application of a series of zero-phase Butterworth Filters. Finally, time-variant decibel scaling was applied to the stack to balance the amplitudes in the final section (Fugro Seismic Imaging, Inc., 2012).

The 2D data were collected in the same manner and with the same parameters as the 3D data and processed in a similar manner. The 2D data line spacing of 100 m was too far apart, however, to be included in a 3D volume; 3D processing therefore was not undertaken on these lines. The 2D data were collected at 100 m line spacing with the intent of filling in between these lines at 12.5 m spacing so that a 3D volume could be constructed that would cover the entire planned survey area. However, due to time and weather constraints, only the northern and central areas were surveyed in the density required for the construction of a 3D volume.

### 3.0 METHODOLOGY

This section describes the methods used to interpret the 3D/2D seismic-reflection data. The extent of data collection is shown on Figure 2-2 and described in Section 1.3, above. The post-processed 3D/2D data extend vertically to approximately 500 ms, or 0.50 s (~400 m), with better imaging (interpretability) generally in the upper 350 ms, especially from 0.035 s (~280 m) to 100 ms or 0.10 s (~80 m).

#### 3.1 Team-Based Approach

The interpretation of the 3D/2D data was conducted using a team-based approach with a well-experienced group of geophysicist and geologists. The term interpretation, as used in the analysis and presented in this technical report, is defined as the visual observation and recognition of features or acoustic signals (reflections) in the 3D/2D data set, assisted by standard software used in the geophysical community, industry, government, and academia to characterize 3D/2D seismic-reflection data, and map stratigraphic layers and geologic structures. Each team member initially interpreted the same set of seismic-reflection profiles. These interpretations were then compared to determine differences in interpretive styles and identification of acoustic structures. It is notable that all team members consistently interpreted structures and acoustic anomalies in the same fashion. Successful results from this first stage of interpretations enabled team members to independently interpret and map the 3D/2D data in different parts of the study area, then collaborate to successfully integrate the findings into a collectively supported (consensus) interpretation. A primary objective of the team approach was to minimize the introduction of model-based interpretive bias that could occur should one individual perform all of the interpretations. Additionally, the team approach facilitated a comparison of each member's interpretive style and ability, providing insight into the possible range or alternatives of interpretations, and thus the variability of the geologic conditions imaged by the 3D/2D data.

The interpretation team consisted of the following experts, listed with their key roles:

- Technical Coordinator—Dr. Stuart Nishenko (Seismologist, PG&E)
- Interpretation (Lead Coordinator) and technical report preparer—Dr. H. Gary Greene (Marine Geophysicist/Geologist, Moss Landing Marine Laboratories)
- Interpretation—Michael Angell (Structural Geologist, Fugro Consultants)
- Interpretation—Justin Pearce, Certified Engineering Geologist (CEG; Fugro Consultants)
- Interpretation—Hans AbramsonWard (CEG, Lettis Consultants International)

The interpretation team met regularly to discuss independent interpretations of the seismic-reflection data set (e.g., profiles, time slices) and derivative data sets (e.g., similarity maps), and to develop criteria for mapping structures, promote consistent mapping across the data set, ensure that there was a relatively even distribution of map interpretations within the data set, and ultimately develop consensus interpretations.

The methods of data interpretation were consistent with the geologic and geophysical interpretation of seismic-reflection data outlined by Sheriff (1982), Yilmaz (2001), and Brown (2004). The following interpretation tasks were implemented:

- Mapping of selected stratigraphic layers (reflections, horizons) that are either locally prominent or laterally extensive within the 3D/2D data set, including stratigraphic unconformities.
- Mapping of structural features, including faults, folds, and/or acoustical anomalies.
- Correlation of faults and fold axes from one line to another, and using user-selected slices through the 3D cube to confirm orientation and trends.
- Distinguishing areas of relatively good and poor data interpretability (zones of no reflections or chaotic acoustic returns). Regions of poor interpretability are those for which interpretation is not possible or is inferred (Figure 3-1).

Mapping of selected seismic stratigraphic layers (horizons) provided an initial framework that was used to evaluate patterns of deformation in well-imaged seismic strata, including areas of deformed, but unfaulted, strata. This step was undertaken primarily to distinguish faults, and not for the construction of structural contour or isopach maps.

### **3.2 Interpretation Tools**

Seismic Micro-Technology's (SMT) Kingdom Suite™ (now called IHS Kingdom) software package (Version 8.5) was initially used to view seismic-reflection data but a later version (Version 8.6 hot fix 4) was used in this revision. The software package allows the user to view and map on vertical profiles (3D and 2D data sets, cross sections and user-selected cross sections), as well as on horizontal time slices (3D data set, plan view, user-selected). The vertical cross-sectional profiles and horizontal time slices are primarily displayed as seismic-reflection amplitudes. Some similarity time slices (the presentation of similar acoustic characteristics such as waveforms) generated in SMT also are displayed.

Fugro Seismic Imaging (2012) developed seismic attribute (i.e., derivative) volumes, commonly referred to as cubes and obtained from the time-amplitude 3D data set, using SMT. Seismic attributes (e.g., waveforms) are derived from the seismic-reflection data and provide information relating to the amplitude, shape, and/or position of the seismic waveform, which is then compared to similar adjacent waveforms. Seismic attributes may reveal features or patterns that otherwise might not be noticed. The similarity time-slice, or derivative, maps show subtle structural features that may not be observable on the amplitude time-slice maps. Derivative maps used in this investigation consist of amplitude and similarity time-slice maps (Foldout A).

Interpretations were performed on each 2D line (at ~100 m line spacing), with emphasis on those 2D lines outside of the 3D data set. Within the 3D data set, mapping was conducted initially on 3D line numbers evenly divisible by 20 to develop an overall understanding of the data set. In areas having complicated fault geometry, interpretations

were made on either every 5th or every 10th line, as appropriate. In some cases, interpretations were made on every other line to better define continuity of a structure or feature. User-selected profiles provided different apparent (oblique to structural trends) and true view angles (perpendicular to structural trends) across features to evaluate and aid in interpretations. Crosslines were interpreted as necessary to develop accurate mapping and interpretation of shallow structures. Numerous time slices, which include data from every inline and crossline profile, also were interpreted.

### **3.3 Interpretation Criteria**

This section describes the criteria used by the interpretation team to develop technically consistent mapping within the 3D/2D data set. Criteria are specific to the geologic features mapped such as horizons (stratigraphic marker beds and unconformities) and structure (faults and folds).

#### **3.3.1 Mapping Horizons (Stratigraphic Beds and Unconformities)**

Selected stratigraphic beds or layers were mapped based on one or more of the following criteria:

- Vertical sequence of distinct low- and high-amplitude reflections, either as a low-high pair (doublets) or as low-high-low or high-low-high triplets.
- Correlation over several hundred meters in lateral extent (Foldout B).

Angular unconformities were mapped based on one or more of the following criteria:

- Presumed younger sediments overlying an angular-eroded surface of tilted/folded older rocks.
- Reflection onlap, downlap, or toplap against upper or lower bounding surfaces, commonly indicating a hiatus in deposition.

#### **3.3.2 Mapping Faults**

Faults were identified based on one or more of the following criteria:

- Abrupt lateral truncation of reflections.
- Displaced, offset, or broken reflections.
- Correlations of offset reflections across a fault plane.
- Direct fault plane reflections.
- Acoustical anomalies (e.g., presence of diffractions, especially at a reflection termination, or presence of laterally short and bright reflections adjacent to a plane that appear as “flags” or contrasting acoustic signals separated by a plane).
- Visible drag and rollover of reflections.
- Loss or substantial decrease in acoustic coherence beneath a fault plane, or distorted dips observed through a fault plane.



A coding scheme (based on colors and a five-digit numbering system) was created and stored on the PG&E 3D/2D SMT Kingdom Suite project to track faults that were interpreted and mapped by the various team members, and to correlate these with previously mapped faults (Table 3-1). The intent of the scheme is to recognize associations within the spatial fault patterns and map preliminary correlations of each fault identified with known fault zones (e.g., HFZ) or groups of faults (e.g., closely spaced, north-south-trending faults). The numbering system provides information on a fault's attitude (orientation, dip, sense of displacement, if any) and allows for tracking of the each member's interpreted faults. Different colors are assigned to clearly associate each mapped structure with the various fault zones or groups shown on Plate 2 and discussed herein. Four different fault zones, four different fault trends, and one set of unassigned faults have been mapped and assigned a unique set of five-digit numbers as shown below (Table 3-1):

**Table 3-1. Numbering System and Colors Used to Distinguish Fault Types and Association with Fault Zones and Groups (Trends) of Faults in the High-Resolution 3D/2D Seismic-Reflection Survey Area Offshore of DCP**

Fault Name or Trend	Five-Digit Code	Color in SMT Project
HFZ	10000	Red
Point Buchon fault zone	20000	Blue
Western plays of Point Buchon fault zone	30000	Dark green
East Branch Point Buchon fault zone	40000	Gold
N-S-trending faults	50000	Light green
NW-SE-trending faults	60000	Maroon
E-W-trending faults	70000	Pink
Other faults	80000	Violet/purple
Unassigned faults	No numbers	Black

The five-digit code is generated as follows:

- First digit—Name or trend of main trace of fault.
- Second digit—Differentiates a primary strand (digit equals zero) from a secondary strand of a fault zone or group of faults (digit equal to or greater than 1).
- Third digit—Fault attitude and direction of movement.
  - 0 = Strike-slip—vertical to near-vertical fault
  - 1 = Normal—east-dipping, or down on east
  - 2 = Normal—west-dipping, or down on west
  - 3 = Reverse—east-dipping, or up on east
  - 4 = Reverse—west-dipping, or up on west
  - 5 = Uncertain—data interpretability is not sufficient to resolve
- Fourth and fifth digits—Individual fault ID number (up to 99 faults can be listed).

Faults that are continuous and change in dip along strike are given different numbered fault codes along those segments that dip differently.

The code for the eight fault zones and fault trends, plus the unassigned faults, and the colors assigned in the SMT project are presented in Table 3-1. By this code, for example, a west-dipping reverse fault, mapped as a secondary strand of the HFZ, would be written as “12401.”

The numbering scheme represents the team’s current interpretation of isolated faults and those that are associated with fault zones, based on the spatial patterns of the faults. The fault numbering code does not necessarily represent the final fault names, as the initial interpretations presented in this report may change once additional data (e.g., seismicity, gravity, magnetic, or deep-penetration seismic-reflection profiles) are considered. Any future changes made to the coding of the faults will be recorded and explained.

Fold axes were identified and mapped based on one or more of the following criteria:

- Both limbs of a fold are present, or, in the case of a monocline, beds consistently dip one direction.
- The amplitude of the fold is greater than several tens of milliseconds (~20 m).
- The greatest curvature of a sequence in upturned or downturned reflectors.

## 4.0 ASSUMPTIONS

Assumptions that were initially made concerning the adequacy of QA/QC oversight of data collection and processing are presented below. Ultimately, however, PG&E's QA/QC validation of these assumptions was completed and used for this report (see Appendix A).

1. The 3D/2D seismic data were acquired and processed to the standards specified in the survey data reports (Fugro Consultants, 2012a, 2012b) and seismic data processing report (Fugro Seismic Imaging, 2012). It was assumed that QC requirements, as stated in the reports, were rigorously applied.
2. The previous studies by PG&E (2011a, 2011b) of the Shoreline fault zone are acceptable for use in this report based upon its approval by the U.S. Nuclear Regulatory Commission (NRC).
3. Navigational accuracy was consistent with guidelines specified in NCS SubSea Navigation Final Report J00344-FR-001 DCP.P 3D Geophysical Survey Job Documents (NCS SubSea, 2011). This assumption is supported where georeferenced data sets overlap, showing the same structures within the limits of each survey data set (Figure 4-1).
4. All seismic stratigraphy imaged by the low-energy data is assumed to have an average bedrock velocity range of 1,600–1,650 m/s (see Figure 1-3). This velocity range was used when converting time to depth and for estimating depths and inclinations (dips). It is based on a seismic source frequency spectrum (Figure 1-3) and the processing parameters (NMO correction using a brute velocity function of 1,600 m/s applied to the seismic data in the CDP domain) used by Fugro Consultants (2011a, 2011b) in the processing of the seismic-reflection data. This assumption provides reasonable estimated depth calculations to approximately 400 m. Faster velocities would, however, be expected at greater depths.
5. MBES bathymetric data collected and processed (2 m grids, with  $\sim\pm 1$  m resolution) by the Seafloor Mapping Lab of California State University, Monterey Bay, were maintained at International Hydrographic Organization (IHO) S-44 Special Order specifications. Across the entire MBES swath, an average of 95.8 percent of crossline soundings fall within IHO Special Order tolerances, with 99.7 percent within IHO Order 1 (P. Iampietro, pers. comm. to S. Nishenko, 2010; PG&E Multibeam Bathymetry Survey 2009 Quality Control Report, Appendix F of PG&E, 2011b; CSUMB Seafloor Mapping Lab, 2007)). This assumption is validated through the comparison of various geophysical data sets, including the 3D/2D seismic-reflection data that precisely overlie each other as a georeferenced product (Figure 4-1; see Appendix A).
6. The seismic-reflection data used in the Long Term Seismic Program report ("LTSP Report"; PG&E, 1988) were collected to previously acceptable industry standards.

7. The USGS 2D seismic-reflection profiles (Sliter et al., 2009) were collected using industry and scientific standards.

## 5.0 SOFTWARE

The primary software programs used for the analysis and interpretation of the 3D and 2D seismic-reflection data are Seismic Processing Workshop (SPW), UNISEIS, IHS Kingdom, Rock Solid Attributes (RSA), and ArcGIS. SPW was used by Fugro Seismic Imaging to process the 2D seismic-reflection data and UNISEIS, Fugro Seismic Imaging's proprietary program, was used to process the 3D seismic-reflection data. IHS Kingdom is a PC-based program for analysis and interpretation of seismic-reflection data. Version 8.6 was used in this study. IHS Kingdom was used in the interpretation and construction of structure maps, cross sections, and time slices. RSA is a separate program (or module) that provides additional data analysis and visualization capabilities in IHS Kingdom. Similarity time slices from RSA were compared to amplitude time slices from IHS Kingdom. Corroboration of the data interpretations in the validated version of IHS Kingdom (Version 8.6 Hotfix 4) is documented in Appendix A, along with data from RSA that was used on selected figures; software validations for SPW, UNISEIS, and IHS Kingdom; and qualification of the data processed using SPW and UNISEIS.

ArcGIS Version 10, developed by ESRI, is a software package in widespread use by industry, government, and academia that is commonly used to collate and map spatial data in an accurate, georeferenced manner. This software was used to construct maps presented in the Shoreline Fault Zone Report (PG&E, 2011b), some of which are reproduced in this report, as well as maps (plates and figures) used for presentation purposes only. Previously interpreted geologic and structure maps from PG&E (2011b) were used as base maps in ArcGIS for comparison purposes. No calculations were performed on the data using ArcGIS. Therefore, ArcGIS was not validated under NQA.

## **6.0 INTERPRETATION AND ANALYSIS**

The interpretation and analyses of the low-energy, high-resolution 3D/2D seismic-reflection data were compared with previously mapped geology described in the Shoreline Fault Zone Report (PG&E, 2011b). Key observations and interpretations of the data are presented in Section 6.1, and analyses of the implications of these observations for characterizing faults are discussed in Section 6.2.

### **6.1 Interpretation**

Interpretations of the strata and structure were made from a 3D volume and 2D seismic-reflection profiles. The volume was viewed in vertical profiles (consisting of inlines, crosslines, and user-selected lines) and horizontal time slices. Consensus interpretations are compiled and mapped on Plate 2. Data examples illustrating relevant findings are presented on figures of cross-sectional profiles and various time slices in plan view.

As discussed above, the seismic-reflection profiles used in the 2D interpretations and the construction of 3D volume were collected in an identical manner and similarly processed (see Fugro Consultants, 2012a, 2012b; Fugro Seismic Imaging, 2012). The difference between the 3D and 2D data sets is primarily the line spacing and the more sophisticated processing needed to produce the 3D volume. The 3D lines, spaced 12.5 m apart, were necessary for the production of a 3D volume. The 2D lines, at 100 m spacing, are too far apart to permit construction of a 3D volume. Therefore, the 2D seismic-reflection profiles were interpreted without the benefit of horizontal time slices and user-selected cross sections.

#### **6.1.1 Interpretability of Data**

The variability in lithology and water depth and the occurrence and rugosity of bedrock seafloor exposures result in zones of variable interpretability. In zones where acoustic energy is either scattered or absorbed, resulting acoustic returns are typically opaque or chaotic, making them difficult or impossible to use for interpreting geologic structures. Alternatively, in zones where the energy is reflected in a conformable manner, resulting records show relatively coherent reflections, facilitating interpretation. To provide insight into the uncertainties of the 3D/2D interpretations, zones of poor and good data interpretability are color shaded (Figure 3-1; Plate 2). The boundaries between the poor and good interpretability zones are generally controlled by structure (e.g., faults). The criteria used for defining these zones are described in the following sections.

##### **6.1.1.1 Poor Interpretability**

In this report, “interpretability” refers to the expression of seismic reflections in the data as strong or weak, and weak or chaotic reflections are considered to be of “poor interpretability.” The expression of reflections is a function of (1) the type and character of rock imaged by the acoustics (sound), and (2) artifacts or noise in the final 3D/2D data that may be introduced by the seismic-reflection survey design or post processing of the seismic data. With respect to (1) above, seismic-reflection data typically are better suited to imaging bedded sedimentary units than crystalline rock or massive sedimentary units.

In bedded sedimentary units, the impedance contrasts are inherently stronger between beds of sedimentary rocks. Crystalline rock or massive sedimentary units generally do not have planar internal seismic reflections, and thus generally produce zones of “poor data interpretability.” As an example, massive sandstone may have undergone fold-related deformation, but this may not be expressed in a seismic-reflection profile because of a lack of internal planar surfaces (such as bedding or cleavage) that would have localized the deformation. Similarly, highly deformed or steeply dipping reflections (beds) also are difficult to interpret.

The 3D/2D data are characterized as having poor data interpretability in most of the eastern and shallower water-depth parts of the study area, particularly adjacent to bedrock outcrops (Plate 2; Figure 3-1). Other smaller regions of poor data interpretability are located adjacent to, and among, various strands of the HFZ (Plate 2). Within these regions, reflections are generally discontinuous or not recognizable in most profiles and time slices. Faults mapped within these regions are generally inferred from lineaments evident in some time slices, lateral continuity of acoustic anomalies in adjacent profiles, and alignment with the projections of structures mapped elsewhere. As a result, the interpretation and mapping of faults in these regions have varying degrees of uncertainty.

Areas of poor data interpretability were identified based on one or more of the following criteria:

- Relatively chaotic acoustic character (Figure 3-1).
- Abrupt loss of lateral acoustic quality (Figure 3-1).
- Parabolic effects and artifacts (Figure 6-1).
- Bedding “ray” effects and artifacts from upturned beds (Figure 6-1).

In the seismic-reflection profiles, it is more difficult to interpret structure and stratigraphy in two areas: (1) at depth, and (2) in shallow areas where bedrock is exposed because strong seafloor reflections mask weaker deep reflections. Poor interpretability areas also are located where poor acoustically responsive rock types (e.g., highly fractured or heterogeneous rock) occur.

For many of the faults mapped within zones of poor interpretability, *interpretation uncertainty* exists. This uncertainty results from the inability to determine if an observed anomaly or lineament may be the acoustic expression of a fault or some other alternative interpretation, such as a resistant bed or a geologic contact. If numerous acoustic anomalies or lineaments exist in a region, interpretation uncertainty also may include ambiguity in the correlation of individual anomalies or lineaments along strike from one line to another. If a feature cannot be correlated across two to three lines, then its presence and location are uncertain.

An interpretive *measurement uncertainty* is the uncertainty of the mapped position and geometry of a fault or fold. Uncertainty in the interpreted position of a fault or fold is based on the width and variability of the lineament or acoustic anomaly used to interpret the structure. The measurement uncertainty in the position of faults mapped within the zones of poor data interpretability is estimated to range to approximately  $\pm 50$  m horizontally. This range was estimated from the variability in reflections imaged on the

seismic-reflection profiles and the line spacing (100 m for 2D and 12.5 m for 3D profiles) across which a structure could be confidently mapped. Following the criteria described in Section 3.3, faults are mapped as vertical unless fault dip is clearly evident in the seismic-reflection profiles.

As significant uncertainties are associated with the mapping of faults in zones of poor data interpretability, most faults mapped within these zones are shown on Plate 2 as dashed and queried lines, indicating they are approximately located and inferred.

#### 6.1.1.2 Good Interpretability

The 3D/2D data exhibited good data interpretability in most of the western and deeper water depths. Folded sedimentary rocks underlie those parts of the study area situated east of the HFZ. Within these areas, reflections are readily identifiable and commonly may be traced for kilometers, facilitating the interpretation of fold axes and the presence or absence of faults. Faults are interpreted based on abrupt lateral truncation of reflections and by displaced, offset, or broken reflections. Correlations of offset reflections with similar characteristics also are possible across many fault planes. These correlations could be used in the measurement of vertical separation once reflections are correlated and horizontal separation once suitable piercing points are established. Similarly, where continuous reflections are observed to cross the projection of a fault mapped elsewhere, the continuity of reflections may be used to limit the potential length of that fault, and provide information about viable geometric connections among faults in the study areas. Faults mapped within the zones of good data interpretability are typically associated with much less interpretation uncertainty than those mapped in zones of poor data interpretability. Uncertainty in the position of faults in these zones is estimated to be approximately  $\pm 25$  m, as a structure may be mapped with confidence across two lines spaced at 12.5 m apart. Faults and structures in the zones of good interpretability that are based on well-defined lineaments evident in time slices, and that correlate well to other faults, are mapped as well defined and shown as solid lines on Plate 2.

#### 6.1.2 Stratigraphy

This section addresses the acoustic stratigraphy observed in the 3D/2D data set. Six basic seismic stratigraphic features and units are identified:

1. Seafloor.
2. Surficial unconsolidated sediment layer.
3. Unconformity on top of rock, including buried wave-cut platforms.
4. Stratigraphic marker beds in the Tertiary rocks.
5. Unconformities within the Tertiary section.
6. Top of Mesozoic basement.

The seafloor is a distinctly recognizable feature in the 3D and 2D data. The seafloor horizon is mapped as the first high-amplitude reflection encountered directly beneath the water bottom (e.g., Figures 2-5, 6-1, and 6-2a). Vertical bathymetric relief of the seafloor horizon (as mapped) is commonly associated with the rugged bedrock at the seafloor and the margins of mobile sand sheets (Figure 6-2). The sand sheets exhibit relief of up to



1 m locally, and this relief is similarly reflected in the seafloor horizon among cross-sectional views. Hence, apparent bathymetric steps in the seafloor from migrating sand may be expressed as a lineament or tonal contrast in the plan view in the MBES bathymetric image, rather than as a flat homogeneous tonal feature (Figure 6-2b). Mapping the seafloor horizon provides a marker for evaluating any possible seafloor expression of a fault, as well as paleogeomorphic features such as paleo-sea cliffs.

In the Point Buchon to Lions Rock offshore area, a package of thin (<1 m thick) mobile sand sheets is imaged in the MBES bathymetry along a zone that extends from the outer margin of the exposed eroded bedrock platform to the HFZ further offshore (Plate 1). These sand sheets exhibit a distinct morphology of a dune form, with sharp distinct downdrift (lee side) lobe fronts and gradational less distinct up-current (stoss) side margins. Scour-like depressions are interspersed with the sand sheets.

Stringers of sand and gravel fill crevices and fractures in the extensive bedrock outcrops exposed on the inner continental shelf and nearshore areas east of the western boundary of the bedrock outcrops. However, the most prominent unconsolidated sediment packages in the study area are the late Pleistocene and Holocene sediments and the extensive mobile sand sheets that cover much of the central and outer continental shelf. These sand sheets are separated by rippled scour depressions (as observed from USGS camera drops, B. Edwards, pers. comm., 2009) that are floored by gravels or smooth bedrock surfaces. From the 3D seismic-reflection profiles, it is evident that, together with the underlying late Pleistocene and Holocene unconsolidated sediment, many of the sand sheets cover irregular, differentially eroded sedimentary bedrock. Within this bedrock, the more resistant beds project up into the overlying sediments (Figure 6-2a) and may be confused with evidence of faulting expressed on the bedrock surface. These more resistant beds, along with other bedrock relief, appear to locally dam and stabilize the basal part of the mobile sand sheets. Commonly, the fronts of the sheets mimic pronounced bedrock relief, especially in areas where the bedrock feature is perpendicular or sub-perpendicular to the sediment transport direction. To determine if faulting does occur in these confused areas, a bedrock surface map has been constructed by digitally removing reflections that represent the overlying sediments (see Figure 6-3).

Wave-cut platforms on Tertiary and older rock are recognizable in both the 3D and 2D seismic-reflection profiles as sub-planar and gently west-dipping reflections directly beneath the acoustically transparent surficial unconsolidated sediment. Although these features are not the focus of the report, they are described because they are prominent in the data and characteristic of the study area. An example of a wave-cut platform is shown on Figure 6-1. Wave-cut platforms have been previously investigated in the study region (PG&E, 2011b, Appendix I, "Identification, Mapping and Analysis of Offshore Wave-Cut Platforms and Strandlines (Paleoshorelines) in the Shoreline Fault Zone Study Area"). It is anticipated that results from this survey will be integrated into a later report on the subject and used to augment previous investigations.

Much of the bedrock exposed at the seafloor in the study area was identified as Tertiary sedimentary rocks in the Shoreline Fault Zone Report (Section 5.2.1 of PG&E, 2011b; Plate 1). Specific imaged stratigraphic layers have not yet been correlated to specific

known formations, members, or beds in either shallow water or deep water because of an absence of direct geologic data (i.e., drill cores). Within the extent of 3D/2D data coverage, selected horizons in Tertiary bedrock were mapped to establish stratigraphic horizons (beds) that are relatively widespread across the study area. An example of the extent and character of several laterally continuous horizons, as imaged in 3D seismic-reflection profiles, is shown on Foldout B. The correlation of the various horizons, arbitrarily numbered horizon H05 through horizon H40, to onshore geologic units is unknown and, at the time this report was first written, age correlation of the horizons had not been made. However, these marker horizons are notably displaced in some locations but are conspicuously unbroken in other locations (Foldout B). These marker horizons are relevant to estimating offsets and possible long-term slip rates, but they were not used for this report because of the uncertainties regarding their stratigraphic assignment and age. More work is needed to correlate the many horizons observed in the seismic-reflection profiles used in this report to known age markers identified in other reports (PG&E, 2013, 2014).

Several unconformities are imaged in the 3D/2D data. In addition to wave-cut platforms (described earlier in this section), angular unconformities are present within the Tertiary section (e.g., horizon H35 in Foldout B). However, their regional extent and geologic relationship with known stratigraphic formations are not yet established. Furthermore, no attempt has been made to correlate these unconformities to the angular unconformities in the Tertiary sedimentary rocks that were previously mapped and assigned ages as reported by PG&E (1988) and Willingham et al. (2013). Moreover, the unconformities were not systematically mapped for this study. Preliminary analysis of unconformities present in sedimentary deposits west of the primary western trace of the HFZ, however, suggests an unknown component of vertical displacements along this fault (e.g., see Foldout C). Systematic and complete mapping and analysis of the unconformities may yield information to help evaluate timing of late Cenozoic deformation periods.

The contact between the top of Mesozoic “basement” and Tertiary strata is difficult to identify in the 3D/2D data, probably due to the combined effects of decreasing interpretability with depth in the seismic profiles and potentially low velocity contrasts across lithologic contacts. Generally, Mesozoic basement (e.g., Cretaceous sandstone or Franciscan Complex rocks) in lateral contact with Tertiary sedimentary rock at the bedrock surface does not produce a distinct sharp or abrupt marker that can be used to define the depth below the Tertiary sequence and dip of the contact. A lateral change in acoustic signal (e.g., increase in reflections) is observed locally, but does not necessarily mark a lithologic contact or boundary (Figure 3-1a).

### **6.1.3 Structure**

Plate 2 shows folds and faults initially identified and mapped in the study area based on the interpretations of the 3D/2D LESS seismic-reflection profiles in conjunction with the MBES bathymetry and older deep-penetration (CDP) seismic-reflection profiles. These interpretations represent the current consensus of the structures in the study area. A comparison of the current structural mapping with previous interpretations of offshore structural trends is presented on Plate 3. Previous interpretations were based on seismic-

reflection data and onshore and offshore geologic mapping as described in the Shoreline Fault Zone Report (PG&E, 2011b).

The faults and folds mapped in the study area are divided into the following structural components:

- Major long-length (likely on the order of hundreds of meters to kilometers) faults of the HFZ.
- Other long-length (likely on the order of hundreds of meters to kilometers), fairly continuous faults (Point Buchon fault zone).
- Moderate-length (likely on the order of several tens of meters to kilometers), discontinuous faults that splay from the Hosgri and Point Buchon fault zones.
- Minor faults with short lengths that are related to specific larger faults and folds (north-trending and east-trending).
- Minor faults associated with small, intra-formational deformation.
- A prominent, fairly continuous northwest-southeast-trending syncline/anticline pair that lies above the deeper northern Shoreline seismicity sublineament of PG&E (2011b) and a monocline that strikes northeast-southwest.

## 6.2 Analysis

The overall geologic structure within the study area consists of the northwest-southeast-trending HFZ on the west, the Point Buchon fault zone on the east, and a zone of distributed deformation characterized by discontinuous faulting and folding between these fault zones (Plate 2). West of the HFZ, in the offshore Santa Maria Basin, the seismic reflections are relatively flat-lying to gently west-dipping in attitude. East of the HFZ, on the continental shelf, well-imaged seismic reflections are gently deformed into a system of folds that trend northwest across the majority of the study area. In the northern part of the study area, this system of folds transitions into a northeast-trending, north-dipping monocline.

Several additional minor faults are identified within the data set. These faults typically extend only a few tens of meters in plan view and are localized within the folded strata east of the HFZ (Foldout B). They may be acoustic anomalies rather than true faults, as they appear to be aligned along the data collection tracklines and anomalous stripping observed in various time slices. Not all potential intra-formational faults were mapped, as the team concentrated on defining and mapping the more prominent continuous and better defined faults.

There are broad areas that are acoustically opaque and/or contain distorted reflections that hamper interpretability, particularly in the eastern part of the study area (Plate 2). Based on sharp contrasts or differing acoustic signatures to the north, the zone of poor interpretability is bounded by, and in some places coincides with, the East Branch and western splays of the Point Buchon fault zone (Figure 3-1b; Plate 2). In the central area, the poor interpretability zone is more complex and lies between Point Buchon fault zone and the coded 30000 series fault splays. In the central part of the study area, the zones of poor interpretability lie between the western splays of the Point Buchon fault zone and a

broad anticline, and in the southeastern part of the 2D survey area, they coincide with areas where bedrock is exposed at or near the seafloor.

The following sections describe the locations, extents, geometries, and geometric connections of faults in the study area (Plate 2). Where possible, the sense of displacement and/or relative direction of vertical fault separation is given.

### **6.2.1 Hosgri Fault Zone**

The HFZ is the most prominent continuous and complex fault zone in the region. Previous mapping (PG&E, 1988; Willingham et al., 2013) of this structure in the area offshore of Point Buchon indicates that the structure consists of a zone of faults that generally coincides with the shelf break. Previous detailed mapping of this part of the HFZ indicated that it is an active transpressional right-slip fault zone (Plates 1 and 3a). The previous mapping was based on the interpretation of high-resolution 2D seismic-reflection profiles spaced approximately 800 m apart that were collected by the USGS in 2008 and 2009 (Sliter et al., 2009) and reported in the Shoreline Fault Zone Report (PG&E, 2011b). As shown by PG&E (2011b), the HFZ generally consists of three to four major strands and associated subparallel splays within a zone that ranges in width from approximately 1 to 2.5 km. The fault zone trends northwest-southeast ( $\sim N25-30^\circ W$ ); however, traces within the fault zone exhibit a left-restraining bend to the south and west of the study area (Plate 3a). Earthquake focal mechanisms along the HFZ are consistent with right-lateral strike-slip motion on steep northeast-dipping faults (see Figure 6-10, Section 6; Hardebeck, 2010, 2012, 2013).

Interpretation of the 3D/2D data reveal that the geometry of the HFZ within the shallow section is more complex than previously mapped (PG&E, 2011b), and it is slightly different from the geometry that was previously interpreted. This increased complexity is now recognized because the reduced line spacing of the 2D survey (i.e., 100 m for the current survey compared to 800 m for the previous USGS surveys) and the availability of the 3D volume for part of the area permit a much more detailed examination of the fault zone. As currently mapped, the HFZ consists of a relatively simple linear zone of faults in the center of the study area that spread out into more diffuse and complex zones of faults in both the northern and southern parts of the study area (Plate 2). Many of the strands within the fault zone are restricted to the Tertiary sedimentary bedrock sequence (Foldout C) identified previously in the PG&E Shoreline fault zone study (PG&E, 2011b). However, some strands extend to the bedrock surface and are buried beneath surficial sediment, whereas others extend to the seafloor (Figure 6-4), cutting the Quaternary sedimentary package.

#### **6.2.1.1 Northern Part of Study Area**

The HFZ at the northern end of the study area steps to the right and forms an extensional or releasing bend that is expressed as a system of faults that bound a small ( $\sim 375$  m wide) graben (Foldout C), herein called Graben A. Faults along the inferred western margin of this graben (faults coded 10005 and 11205) are approximately aligned with the primary strands of the HFZ in the southern and central parts of the study area (e.g., fault coded

10002 shown on Plate 2 and discussed in more detail in this section and in Section 6.2.1.2 below). The faults that bound the eastern margin of the graben (faults coded 11006, 11208) separate gently dipping and folded reflections (probably Pliocene Miguelito Member of the Pismo Formation) from faulted well-layered graben-fill sediment of unknown age (Foldout C).

West of the faults bounding Graben A, another set of north-trending normal faults (the coded 50000 series faults) is observed in the 3D/2D data. These include both east-dipping and west-dipping faults that typically exhibit normal displacements within a sequence of relatively flat-lying reflections. Three of these faults (faults coded 51202, 51203, and 51111) extend upward to an unconformity that occurs approximately 0.03 s (~24 m) below the seafloor (Foldout C). At least one of the faults (fault coded 51202) appears to disrupt this unconformity. This unconformity is shown at a depth of approximately 0.16 s (~128 m) below the 0 datum, which is approximately sea level, on Foldout C. These faults occur at about the same location as the previously mapped western strand HFZ Trace A2 (PG&E, 2011b; Plate 3a).

In the northern part of the 3D survey block, the HFZ is characterized by a single dominant fault strand (fault coded 10002), which locally is accompanied by associated secondary splays (Plate 2). The primary strand is acoustically defined by the distinct truncation of folded reflections on the east with flat-lying reflections on the west (Figure 6-4). Locally in the northwestern part of the 3D survey area, bedrock is elevated as a northwest-southeast linear ridge (pressure ridge) projecting above the sediment-covered seafloor. The pressure ridge is bounded by faults having seafloor expression, including a fault coded 10002 on the west and a secondary splay of the HFZ (fault coded 11003) that splits and bounds the ridge on the east (Figure 6-5). As shown on Figure 6-4, chaotic acoustic reflectors are present between the central and eastern faults in the profile, in contrast to more organized and coherent reflections on the opposite sides of the faults.

Another secondary splay, fault coded 11001, lies approximately 20–30 m west of the primary strand, and is buried approximately 0.05 s (40 m) beneath the seafloor (Figure 6-4). As shown on the figure, “bright spots” of folded and truncated reflections are imaged along the west fault and in a synclinal fold between the two westernmost faults of this strand. The bright spots most likely represent gas-charged sediments, where gas migrating up along the faults has been trapped. Fault coded 11001 is a persistent feature in the northern part of the 3D survey, and also in the 2D profiles to the north, running parallel to the primary fault coded 10002 for a distance of approximately 1.4 km.

South of the pressure ridge, fault coded 10002 extends to within a few milliseconds (a few meters) of the seafloor (the upward termination of the fault strand in profiles is obscured by the bubble pulse), but no seafloor scarp is evident in the MBES image near the upward projection of this fault (Plate 2). This fault extends southward beyond the limit of 3D data set, and is expressed in 2D profiles in the shallow subsurface as a single fault that truncates steeply dipping, well-defined parallel reflections on the east and an acoustically opaque zone on the west. The fault appears to extend into and displace unconsolidated Quaternary sediment beneath the seafloor.

The 3D data indicate that, within the shallow section, no throughgoing strand of the HFZ exists to the east of fault coded 10002. At depth, other faults exist, such as those that comprise the Hosgri thrust fault system, but others are difficult to define as acoustic “wipe-outs” from shallow-lying gas-charged sedimentary layers may be masking deep structure and stratigraphy. East of faults coded 10002 and 11003 is a sequence of steeply dipping and locally tightly folded, relatively thin-banded reflections (Figure 6-4). These reflections cross the previously mapped location of Trace C2 of the HFZ and are not faulted, indicating that Trace C2 either does not extend into the uppermost 200 m of section or does not exist at this location (Plate 3).

#### 6.2.1.2 Southern Part of Study Area

South of fault coded 10002, the HFZ widens and becomes more disorganized (fragmented or less continuous) with several strands splaying to the east in the region where the 3D/2D survey areas meet. This behavior could, however, be the result of less resolution in the spacing of the seismic-reflection survey lines (Plate 2). Numerous subparallel, discontinuous faults that strike approximately N20°-40°W, most of which are only a few hundred meters in length, can be correlated on only a few adjacent seismic profiles. In the southernmost part of the study area, traces of the HFZ strike distinctly more westward, approximately N40°-70°W and extend approximately parallel to the strikes of fold axes and bedding inferred from the MBES bathymetry (Plate 3).

In contrast to the sharp juxtaposition of folded reflections against relatively flat-lying reflections associated with fault coded 10002 (in the north), the acoustic stratigraphy and structure evident in the 2D seismic-reflection profiles in the southwestern part of the study area become choppy in appearance. More and tighter folding is present to the east, whereas to the west the folds are broader and gently dipping. Outcrops of bedrock are evident in MBES imagery in the southwestern part of the study area, suggesting that surficial sediments are thin, and that the rocky part of the continental shelf extends west of the study area.

#### 6.2.2 Point Buchon Fault Zone

The Point Buchon fault zone is a structurally complex feature that cuts through and deforms Tertiary strata in the central and northern part of the study area. This fault zone is well defined on Plate 2 and its component structures are described below:

- The main trace is a continuous linear fault that extends northwest from the southeast corner of the 3D survey to near the northern end of the study area where a graben, herein called Graben B, has been mapped. This fault zone includes the faults coded in the 20000 series and individual faults coded 40001, 40003, and 40002 and may also include shorter, less well-defined faults mapped along the same trend to the southeast (Plate 2).
- An east branch that splits from the primary fault at the southern end of fault coded 40001 extends northwestward beyond the northern limit of the 3D study area. This branch also includes other faults coded in the 40000 series.

- Several short faults that splay westward from the main fault trace in the center part of the study area (the coded 30000 series faults).

The Point Buchon fault zone is characterized in the 3D/2D LESS, MBES, and older CDP data sets. Good correlation between the LESS and MBES data, even in areas of poor seismic-reflection interpretability, allow for confident mapping of this structure (Figures 3-1 and 4-1).

Parts of the Point Buchon fault zone that were originally described as the N40°W fault zone in the Shoreline Fault Zone Report (PG&E, 2011b) were mapped as a less complex fault zone than interpreted herein. These include the southern part of the main trace of the Point Buchon fault zone and associated faults, which trend approximately N45°W, and the East Branch of the Point Buchon fault zone, which trends approximately N35°W (Plate 2).

#### 6.2.2.1 Main Trace of Point Buchon Fault Zone

The south end of the Point Buchon fault zone bounds exposed rock on the seafloor that is characterized by poor data interpretability in areas of seafloor bedrock exposures and gas masking (Plate 2). Seafloor geology reported in PG&E (2011b) indicates that the fault zone in this area consists of up to two closely spaced (i.e., up to ~150 m apart), discrete fault traces that locally are associated with distinct seafloor bedrock scarps (Plate 1). The fault separates relatively resistant blocky Obispo Formation on the east from a less blocky rock type on the west, probably of the same formation (Plates 1 and 3b).

The main trace of the Point Buchon fault zone is expressed in the seismic-reflection profiles as an acoustic anomaly and abrupt change in acoustic character from one side of the fault to the other. However, time slices from the 3D amplitude volume show the fault as a continuous sharp lineament within an acoustical chaotic zone, which coincides with the well-imaged bathymetric scarp along the coded 40000 series faults, specifically the fault coded 40003 (Figures 6-5 and 6-6; Plate 3b). South of the bedrock exposure, the fault zone trends toward, and may converge with, the central segment of the Shoreline fault zone, although a direct connection could not be identified within this zone of poor data interpretability (Plate 2).

The north end of the main trace of the Point Buchon fault zone is shown to continue as a fairly linear fault zone buried beneath surficial Quaternary sediments (Foldout D). Acoustically, for most of its length, the structure is characterized as a narrow zone of chaotically disrupted and offset reflections to the east that are truncated against well-imaged, gently dipping reflections to the west (Foldout Db).

The northwestern end of the Point Buchon fault zone widens and includes north- and northwest-trending faults (on Figure 6-7 from left to right, faults coded 21101, 21201, 21202) that exhibit normal displacement. These faults, along with fault coded 20005, bound and cut Graben B. These faults separate folded and dipping reflections of probable Tertiary sedimentary rock from thinly bedded, seafloor-parallel to subparallel acoustic layers that probably represent graben fill. The age of the probable graben-fill sediment is unknown. However, the graben-filling reflections are nearly parallel to the seafloor and

are bounded by Tertiary bedrock, suggesting that the graben-fill sediment may be significantly younger than the surrounding materials, possibly Quaternary to Holocene in age (i.e.,  $< \sim 2.6$  Ma).

The lowermost part of the graben-fill sequence is offset by faults in the Point Buchon fault zone. The northwest end of the graben appears to be truncated by a north-south-trending fault (fault coded 11008) that exhibits displacement down to the east. This fault is parallel to, and may be part of, a set of normal faults that branch northward from the central trace (fault coded 10001) of the HFZ and bounds Graben A (described in Section 6.2.1.1 and shown as fault coded 11208 on Figure 6-7b and Plate 2). The total fault length is approximately 7.5 km from the northern end of Graben B (defined by fault coded 11008) to the southern extent of the Point Buchon fault zone (Plate 2).

### 6.2.2.2 East Branch Point Buchon Fault Zone

The East Branch of the Point Buchon fault zone splits northward and east of the main trace of the fault zone at approximately inline number 1480 of the 2D survey (Figure 2-2, Plate 2). It is oriented  $\sim N35^\circ W$  compared to the main trace, which is oriented approximately  $N45^\circ W$ . Much of the East Branch of the Point Buchon fault zone is mapped on the basis of the linear  $N35^\circ W$ -trending seafloor scarp that separates bedrock on the east from unconsolidated sediment on the west (Plate 3b). In the northern part of the 2D study area, north of the 3D survey block, faults along the East Branch are imaged on only a few 2D seismic-reflection profiles and mapped based on bent and truncated acoustic reflections (Figure 3-1a). The faults of this branch may be more continuous at depth, as they lie in areas of poor interpretability and it was not possible to interpret their deeper extent. To the south, in the 3D survey block, the East Branch of the Point Buchon fault zone is exhibited in the 3D/2D data as a narrow zone up to 100 m wide that clearly truncates a broad open syncline on the east and separates this broad fold from a series of folded and disrupted reflections on the west (Foldout D). Here, the fault zone extends vertically to the top of bedrock, but is buried by an acoustical transparent layer of surficial sediment.

The East Branch of the Point Buchon fault zone is approximately 6 km long, and if the main trace of the Point Buchon fault zone within the study area is included, the total length of the fault zone is approximately 9 km. The fault may extend beyond the northern limit of the study area, projecting toward a fault mapped from the 2008/2009 USGS data (Plate 3a) as the easternmost trace of the HFZ. To the south, the Point Buchon fault zone may connect with the central segment of the Shoreline fault zone in the vicinity of Lions Head Rock (Plate 2).

A complex fault intersection occurs where the East Branch of the Point Buchon fault zone (fault coded 40008 on Figure 6-6b) splits from the main fault (fault coded 40001 on Figure 6-6b). Figure 6-6b is a time slice at 74 ms through the 3D similarity volume that shows the faults at this intersection as subtle lineaments (light intensity) cutting through acoustically opaque bedrock (dark intensity). The light intensity lineaments appear to be troughs in the top of bedrock that are filled with sediment resulting from differential erosion into bedrock (dark areas) along the faults. Other faults (the coded 31000 series



faults) can be seen in the time slice splaying northwestward from the main trace of the Point Buchon fault zone. These splay faults are discussed in the following section.

### 6.2.2.3 Western Splays of the Point Buchon Fault Zone

A series of four to five generally northwest-trending faults (the coded 30000 series faults) near the center of the main trace of the Point Buchon fault zone splay west from the main fault zone and step to the north in map view (Plates 2 and 3b). These faults range from approximately 0.7 to 1.7 km in length and dip steeply (near-vertical) to the northeast (Figures 6-8 and 6-9). The faults truncate upturned reflections (possibly sedimentary beds) along the eastern limb of a syncline and juxtapose reflection-rich strata on the west against reflection-poor acoustic returns on the east (Figure 6-8a). The amount of displacement and sense of fault slip are therefore not resolvable. Additionally, there appear to be moderate ray effects (piping)/interference (dipoling) on the upturned beds at the bedrock surface, which may be confused with dipping reflections. When viewed on the coast-parallel 3D crosslines, faults within this zone are expressed as northwest-southeast oriented acoustically chaotic zones that range approximately 100–125 m wide.

The splay faults generally bend gently westward near their northern extent and die out in the cores of asymmetric anticlinal folds south of the HFZ. The geometry of the fault-fold relationships of the splay faults suggests they may be associated with wrench tectonics (shear couple in a strike-slip fault regime) and faults of the same age and deformation system (conjugate faults).

### 6.2.3 ***Structures Coincident with the Northern Shoreline Seismicity Sublineament***

This section describes the structural features mapped in the vicinity of the northern Shoreline seismicity sublineament (i.e., the northwest trend of epicenters). As shown on Plates 1 and 3a, surficial structures mapped for the Shoreline Fault Zone Report (PG&E, 2011b) along this alignment include a 6.5 km long, northwest-trending syncline that approximately overlies the seismicity sublineament and three queried near-surface shallowly buried bedrock faults that intersect the axis and eastern limb of the syncline. For the Shoreline Fault Zone Report, these features were inferred to represent one of several alternative interpretations of the location for the north segment of the Shoreline fault zone (PG&E, 2011b).

#### 6.2.3.1 Folds

A major structural element within the 3D/2D study area is an extensive northwest-trending syncline (Plate 2) that uniformly deforms Tertiary strata, and coincides with the northern Shoreline seismicity sublineament mapped and reported by PG&E (2011b). The structural axis of this syncline is almost directly coincident with the synclinal axis interpreted from the USGS seismic-reflection profiles and reported in PG&E (2011b) (Plate 3a). Based on the mapped 3D/2D data, the axis of the syncline appears to step easterly in the southeast direction, consistent with mapping reported in PG&E (2011b). The syncline extends from the southeast part of the study area for over 7 km, where it is

intersected by two north-south-oriented faults (fault coded 51001 and 51301 on Figures 6-8a and 6-9a) that separate this structure from an east-northeast-trending, northwest-dipping monocline (Plates 2 and 3b). The syncline terminates in the northwest and does not connect with the HFZ. Previous mapping (see Plate 1) showed this syncline as a more continuous structure in the vicinity of the HFZ (PG&E, 2011b).

Anticlines, formed along the western limb of the syncline, are mapped directly west of the major syncline described above and are represented by two relatively short (~500 m long), anticlinal axes located directly to the west of the western splays of the Point Buchon fault zone (Plate 2). The anticlinal axes west of the syncline are generally consistent with an anticline mapped and reported in PG&E (2011b; Plate 3a). Close examination of the 3D/2D data indicates that the anticlinal axes are subparallel to the synclinal axis. The Tertiary rocks east of the anticline and west of the syncline are deformed but not faulted.

### 6.2.3.2 Complex Structural Area

The 3D/2D data better resolve the fault geometries (Plate 3b) along and near the easternmost inferred and queried fault trace of the north segment of the Shoreline fault zone than previous interpretations made from the more widely spaced USGS seismic-reflection profiles (PG&E, 2011b; Plate 3a). In this area, a series of four or five generally northwest-trending faults (the coded 30000 series faults on Figures 18a and 19a) splay to the west from the Point Buchon fault zone (Plates 1 and 3a).

The 3D/2D mapping does not show a continuous north segment of the Shoreline fault zone (PG&E, 2011b). However, the 3D/2D data provide evidence for a zone of noncontiguous faults (the 30000 series western splays of the Point Buchon fault zone) that follow the eastern margin of the major syncline discussed in Section 6.2.4. The 3D/2D data generally indicate that these faults are vertical to gently east-dipping in the shallow subsurface. These faults may merge at depth but their geometry is unknown and no evidence of this situation is seen in the shallow penetrations 3D/2D data set. Given the location uncertainty ( $\pm 0.5$  km) of the offshore earthquakes (PG&E, 2011b), the seismicity sublineament may be associated with these merged faults at depth, although no evidence exists for the continuation of these faults below 0.4 km (Plate 3). In other words, the seismicity sublineament may represent the surface expression of the steeply southwest-dipping Point Buchon fault zone, and associated splay faults, rather than the northwest continuation of a vertical Shoreline fault, as originally proposed (Hardebeck, 2010; PG&E, 2011b). Earthquake focal mechanisms in this region exhibit both right-lateral strike-slip motion parallel to the strike of the Hosgri and Point Buchon/ Shoreline fault zones and oblique-slip that is subparallel to the trend of the western splays of the Point Buchon fault zone (see Figure 6-10).

West of the western splays of the main Point Buchon fault zone (the coded 30000 series faults), well-imaged well-layered reflections within the broad syncline are generally uninterrupted by faults (Figure 6-8). Exceptions include two north-trending, east-dipping faults (faults coded 51001 and 51301 on Figure 6-8 and Plate 2) that together offset reflections vertically by approximately 0.01 s (~8 m) up on the east. Based on the loss of

acoustical expression of the fault coded 31301 to the north, it appears that the zone of coded 30000 series faults terminates at a structurally complex location where a monocline meets with the reverse faults, coded 31301 and 71401 (Figures 6-8b and 6-9b).

### 6.2.3.3 Northern Extent of the Shoreline Seismicity Trend at the Hosgri Fault Zone

In the Point Buchon fault zone, the gently north-plunging syncline opens to become a broader fold and is intersected by faults coded series 51000 approximately 600 m south of the northwest extent of the 30000 coded west splay faults (Foldout Bb). The map trace of the syncline axis stops where this broad fold terminates and a northwest-dipping monocline occurs (Plate 2; Foldout Bb). Directly northwest of the monocline axis, reflections dip to the north. In a time-slice amplitude map at 0.150 s (Figure 6-9b), two observations are made:

- Reflections are laterally continuous and not faulted by the easternmost strand of the HFZ as shown on Plate 3a (Trace C2) in this area.
- Reflections are laterally continuous and unbroken directly northwest of the coded 30000 series faults.

Therefore, a shallow (above a depth of 400 m) geometric connection between the HFZ and the proposed north segment of the Shoreline fault zone is not possible as inferred by the northern Shoreline seismicity sublineament on the shallow penetration 3D/2D data set.

The north end of the main trace of the Point Buchon fault zone is divided into many en echelon faults and appears to die out into a fold and cross faults that trend north-south and separate grabens 'A' and 'B' (e.g., fault coded 11008). The East Branch of the Point Buchon fault zone becomes less continuous in the northern study region than directly to the south, within the 3D survey block, and is primarily characterized by en echelon faults and a western splay fault (fault coded 41301) that die out in a zone of extension (Plate 2). The East Branch of the Point Buchon fault zone appears to extend to the north beyond the study area.

## 7.0 CONCLUSIONS

The 3D/2D data set used to evaluate the geology offshore of the DCP.P significantly improves the understanding of regional geologic structure and represents an important contribution to the knowledge base needed for evaluating the seismic hazards. Despite limited acoustic penetration from the low-energy source in some areas, particularly in shallow water depths, and zones of poor interpretability that are present in the data, the 3D/2D data set allows for more detailed mapping than was previously possible. Specifically, the 3D seismic volume and the close spacing of the seismic-reflection profiles permit better correlation of faults and folds to more confidently characterize geology and more accurately determine structural trends and extents. In other words, more complete structural mapping is possible due to the high-resolution and dense line spacing of the 3D/2D data (12.5 m for the 3D survey and 100 m for the 2D survey).

The main structural elements mapped in the study area are the HFZ, the Point Buchon fault zone, and a prominent syncline that deforms Tertiary strata in the southern two-thirds of the study area.

### 7.1 The Hosgri Fault Zone

The HFZ consists of numerous fault strands and is the best imaged and most continuous and complex fault zone in the region. The fault juxtaposes folded Tertiary strata on the east against relatively flat-lying reflections of probable Quaternary age on the west. Locally, strands of the fault zone exhibit seafloor expression, either as erosional fault-line scarps, or as tectonic scarps within young sediment. Several strands of this fault zone are identified in the 3D/2D data set that shows bright spots of associated gas pockets. The 3D/2D data set shows that this fault zone is more complex at depths less than approximately 400 m than previously mapped (PG&E, 1988; PG&E, 2011b) (Plate 3). This increased complexity is recognized primarily because of the high-resolution of the data and small (12.5 m) line spacing of the 3D/2D data (12.5 m for the 3D survey and 100 m for the 2D survey).

In the study area, the local style of faulting changes along strike of the HFZ. Graben A, bounded by right-stepping strands of the HFZ in the north, indicates extensional strike-slip faulting (transtension; Plates 2 and 3b). A single fault strand characterizes the fault zone in the center of the study area. Numerous, relatively short strands fan out to the southeast and are associated with folds in the south, indicating compressional strike-slip faulting (transpression). Similar morphology and structure is observed along many strike-slip fault systems, and various researchers have postulated different terminology and models of formation of such features (e.g., see discussion in Mann, 2007). Reading (1980) reported that along strike-slip fault systems, small-scale alternate zones of extension and compression occur. Reading (1980) states that these zones can occur along the following structures:

- curved parts of strike-slip faults
- braided faults within a strike-slip fault system
- side-stepping, en echelon (conjugate) faults

This pattern has been described for the San Andreas Fault System within the study region (Kingma, 1958; Quennell, 1958; Crowell, 1974; Dickinson, 2004b).

## 7.2 The Point Buchon Fault Zone

The Point Buchon fault zone, northwest of the central segment of the Shoreline fault zone, is a northwest-trending fault that disrupts Tertiary strata east of the HFZ. Segments of the fault zone, including the southern part and the East Branch, were originally mapped as the N40°W fault zone and described in the Shoreline Fault Zone Report (PG&E, 2011b).

Both the main and Eastern Branch of the Point Buchon fault zone exhibit probable fault-line scarps, which are clearly evident in the MBES bathymetric images and subcrop mapping (Plate 2). To the south, the Point Buchon fault zone may connect to the central segment of the Shoreline fault zone and associated structures, although no identifiable connection has been observed in the 3D/2D data.

Approximately halfway along the mapped length of the East Branch of the Point Buchon fault zone, a moderately well-defined narrow zone of faults bifurcates toward the north. Here the East Branch is parallel to the HFZ and likely continues north beyond the study area (Plate 2).

In the northern part of the study area, Graben B is associated with the northern end of the Point Buchon fault zone (Figure 6-7; Plate 2). Although there is no information on the age of the sediment fill in the graben, the occurrence of generally seafloor-parallel and subparallel reflections filling a graben bounded by Tertiary bedrock suggests that the graben-fill sediment may be significantly younger than the surrounding stratigraphy, possibly Quaternary to Holocene in age (i.e., less than ~2.6 Ma). A north-trending fault (fault coded 11008) that may be part of the HFZ truncates this graben at its northwest extent (Plate 2). Graben B is located approximately 400–500 m east of the primary traces of the HFZ. The presence of this graben and Graben A to the northwest is indicative of transtension in the northern part of the study area, but the structural relationship between the two grabens and structures within Estero Bay to the north of the study area needs to be further evaluated.

A system of splay faults branches off to the west of the main Point Buchon fault zone, close to where the East Branch splits from the main trace. These splay faults trend west-northwest and die out in the cores of asymmetric anticlinal folds without observed direct linkage to the shallow (upper 400 m) parts of the HFZ (Figure 6-8).

## 7.3 Folding

The geometry of folding in Tertiary strata indicates a northeast-southwest horizontal direction of maximum shortening. Deformation within the Hosgri and Point Buchon fault zones is predominantly northwest-southeast oriented and representative of a strike-slip fault system (Reading, 1980; Mann, 2007). Minor discontinuous faults generally occur as north- and east-trending sets (Plate 2), and are localized within the Tertiary folded section, indicating they are related to the folding stress field. These minor faults likely are

bending moment faults formed during folding of strata as indicated by bent reflections. Northeast-trending faults exhibiting minor warping of the fold axes suggest that some northeast-southwest-directed tearing might have deformed the folds.

#### **7.4 Northern Shoreline Seismicity Sublineament**

The 3D/2D data set shows several faults in the vicinity of the northern Shoreline seismicity sublineament (as defined by Hardebeck, 2010, and PG&E, 2011b). Two postulated (queried) continuous and linear northwest-trending, en echelon faults along this seismicity trend were reported in the Shoreline Fault Zone Report (PG&E, 2011b) based on the interpretation of widely spaced (800 m) 2D seismic profiles (Plate 3a). The 3D/2D data set more clearly delineates the locations of structures in this area and provides improved imagery of subsurface geology (Plate 3b). The Point Buchon fault zone is located approximately 300–750 m northeast of the surface projection of the northern Shoreline seismicity sublineament (Plate 3b), although the approximately 0.5 km location uncertainty of the earthquakes may reduce this offset. However, no well-defined continuous, throughgoing basement surface faulting that is coincident with the seismicity sublineament was observed to connect directly with the HFZ (Figure 6-3). In other words, the seismicity sublineament may represent the surface expression of the steeply southwest-dipping Point Buchon fault zone and its western splay faults rather than the northwest continuation of a vertical Shoreline fault, as originally proposed (Hardebeck, 2010; PG&E, 2011b).

Four faults that splay westward from the Point Buchon fault zone may overlie the seismicity sublineament. These 30000 series faults on Plate 2 appear to die out to the west in the shallow subsurface (i.e., the uppermost ~50–400 m below the seafloor) without reaching the HFZ. Uninterrupted (unfaulted) reflections are seen in the 3D/2D data to be continuous across parts of the northward projection of the seismicity sublineament (PG&E, 2011b; Plates 2 and 3).

A shallow geometric connection between the HFZ and the proposed north segment of the Shoreline fault zone, as defined by the seismicity sublineament, was not observed in the 3D/2D data set (see Section 6.2.3.3). As seen on Figure 6-3, no surface fault structure aligns with the northern Shoreline seismicity sublineament, in contrast to what has been observed in the central and southern sublineaments (PG&E, 2011b). While the majority of focal mechanisms associated with both the Hosgri and Shoreline faults represent right-lateral strike-slip motion parallel to the strike of these faults, there are a number of mechanisms that trend subparallel to the Point Buchon splay faults that exhibit a reverse-oblique sense of motion (see Figure 6-10).

Instead, faults die out within an area of transtension characterized by Grabens A and B and the monocline in the northern part of the study area.

Figure 7-1 compares LESS imaging depths (<500 m) to the seismicity cross section for the Hosgri and Shoreline fault zones (2–12 km). Since the 3D/2D data are restricted to the shallow subsurface, the mapped surficial faults cannot be confidently extended to the earthquake hypocentral depths. Therefore, no conclusion can be made in regard to these

faults being the source of the earthquakes that constitute the northern Shoreline seismicity sublineament (Plate 3a).

## **7.5 Strike-Slip Tectonic Models**

The change in faulting style from transtension in the northern part of the study area to transpression in the southern part of the study area is a common feature of strike-slip fault systems (Mann, 2007) as discussed in Section 1.2.2. Folding and uplifted bedrock in the southern part of the study area may result from a left transfer of slip between active traces of the right-lateral HFZ. This fault configuration suggests that distinct quadrants of tension (in the north) and compression (in the south) exist with conjugate faults and folds connecting the primary throughgoing faults of the main traces of the HFZ in a fashion described from the mathematical models of Rogers (1980) and clay models of Wilcox et al. (1973). More recent, scaled analog clay model experiments provide additional insights into the structural geometry and evolution of releasing and restraining bends (e.g., McClay and Bonora, 2001; Mitra and Paul, 2011).

Harland (1971) states that folds form at oblique angles to the strike-slip fault in an echelon pattern, though if transpression is dominant, the folds are rotated so that they are subparallel to the fault. Therefore, the Hosgri–Point Buchon fault zones parallel en echelon folds in the central and southern part of the study area, which may be inferred to have resulted from a dominant transpressional regime. En echelon folds have been suggested to indicate deformation in plastic (ductile) cover rocks overlying strike-slip faults in more rigid basement rocks at depth (Reading, 1980). This situation may occur in the study area, although ages of folding are not well constrained and must be determined.

## 8.0 LIMITATIONS

Attachment 7.3 of the PG&E Geosciences Department Procedure CF3.GE2, Quality Related Technical Reports, states “Address any limitations on the use of results and conclusions” of such report. Therefore, in this section we address limitations of the results and conclusions made herein that may be used within other Geosciences reports.

Because the intent of, and the data used for this report is restricted to the shallow subsurface, the use of the results and conclusions presented in this report to characterize structure at depth, especially within the seismogenic zone is limited. Faults mapped in this study were not correlated with faults and microseismicity at depth, as the 3D seismic-reflection acoustics did not penetrate to depths that would have allowed for such a correlation.

Age estimates are based on the most recent global sea-level curves because biostratigraphic, radiometric, or radiocarbon ages were not available, and age uncertainties of applicable sea-level curves were considered in the dating of horizons and structures.



## **9.0 IMPACT EVALUATION**

Attachment 7.3 of the PG&E Geosciences Department Procedure CF3.GE2, Quality Related Technical Reports, states “Provide an evaluation of the impact that the results/conclusions have on other Geosciences documents.” For this report the impact to other Geosciences documents is unknown at this time.

## 10.0 REFERENCES

- Atwater, T.M., 1970. Implications of plate tectonics for the Cenozoic tectonic evolution of western North America, *Geological Society of America Bulletin* **81**: 3513–3536.
- Brown, A.R., 2004. *Interpretation of Three-Dimensional Seismic Data*, American Association of Petroleum Geologists, Memoir 42, 6th Edition, Tulsa, OK, 541 pp
- Burchfiel, B.C., and Stewart, J.H., 1966. ‘Pull-apart’ origin of the central segment of Death Valley, California, *Geological Society of America Bulletin* **77**: 439–442.
- California State University, Monterey Bay (CSUMB) Seafloor Mapping Lab, 2007. 2006-07 Multibeam Bathymetry Survey of Morro Bay and Point Buchon, Center for Integrative Coastal Observation, Research and Education; available at <http://Seafloor.csumb.edu/projects.html>.
- Cloos, E., 1955. Experimental analyses of fracture patterns: *Geological Society of America Bulletin* **66**: 241-256.
- Crowell, J.C., 1974. Origin of late Cenozoic basins in southern California: in Dickinson, W.R. (editor), *Tectonics and Sedimentation*, Society of Economic Paleontologists and Mineralogists Special Publication 22, Tulsa, OK, pp. 190–204.
- Dickinson, W.R., 2004a. Evolution of the North American Cordillera: *Annual Reviews of Earth and Planetary Sciences* **32**: 13–45.
- Dickinson, W.R., 2004b. Kinematics of transrotational tectonism in the California Transverse Ranges and its contribution to cumulative slip along the San Andreas Transform Fault System, PowerPoint presentation; [http://seismo.berkeley.edu/~rallen/teaching/S04\\_SanAndreas/Resources/BlockRotationTransrotationalTectonism.pdf](http://seismo.berkeley.edu/~rallen/teaching/S04_SanAndreas/Resources/BlockRotationTransrotationalTectonism.pdf).
- Dickinson, W.R., Ducea, M., Rosenberg, L.I., Greene, H.G., Graham S.A., Clark, J.C., Weber, G.E., Kidder, S., Ernst, W.G. and Brabb, E.E., 2005. *Net Dextral Slip, Neogene San Gregorio-Hosgri Fault Zone, Coastal California: Geologic Evidence and Tectonic Implications*, Geological Society of America Special Paper 391, 43 pp.
- Fugro Consultants, Inc., 2012a. *Field Operations Report 2010-2011, High-Resolution Marine Survey Offshore Diablo Canyon Power Plant, Central California*, Fugro Project No. 04.B0992017, prepared for PG&E, May, 875 pp.
- Fugro Consultants, Inc., 2013b. *2D Data Processing Report for the 2012 Offshore High-Resolution P-Cable Seismic Reflection Data, Diablo Canyon Power Plant, Central Coastal California Seismic Imaging Project*, Report No. PGEQ-PR-13, Rev0, prepared for PG&E, February, 23 pp.
- Fugro Consultants, Inc., 2012c. *Software Validation of UNISEIS and 3D Data Qualification of 2010-2011 High-Resolution Marine Survey Data, Offshore Diablo Canyon Power Plant, Central Coastal California Seismic Imaging Project*, Report No. PGEQ-PR-03 (Rev0), FSI Project No. 2011-4493, June, 67 pp.

Fugro Consultants, Inc., 2012d. *Software Validation for Seismic Processing Workshop and Qualification of 2010-2011, High-Resolution 2D Marine Seismic Reflection Data, Rev. 1, Offshore Diablo Canyon Power Plant, Central California*, Report No. PGEQ-PR-06 (Rev1), Fugro Project No. 04.B0992017, prepared for PG&E, November, 43 pp.

Fugro Seismic Imaging, Inc., 2012. Seismic Data Processing Report, 3D High-Resolution Marine Survey, California Offshore 2011, Diablo Canyon, prepared for PG&E, May, Rept. No. 2010-4410\_Draft01, 36 pp.

Hanson, K.L., Wesling, J.R., Lettis, W.R., Kelson, K.I., and Mezger, L., 1994. Correlation, ages, and uplift rates of Quaternary marine terraces, south-central California: in Alterman, I.B., McMullen, R.B., Cluff, L.S., and Slemmons, D.B. (editors), *Seismotectonics of the Central California Coast Range*, Geological Society of America Special Paper 292, pp. 45–72.

Hanson, K.L., Lettis, W.R., McLaren, M.K., Savage, W.U., and Hall, N.T., 2004. Style and Rate of Quaternary Deformation of the Hosgri Fault Zone, Offshore South-Central California: in Keller, M.A. (editor), *Evolution of Sedimentary Basins/Offshore Oil and Gas Investigations—Santa Maria Province*, U.S. Geological Survey Bulletin 1995-BB, 33 pp.

Hardebeck, J.L., 2010. Seismotectonics and fault structure of the California central coast, *Bulletin of the Seismological Society of America* **100** (3): 1031–1050, doi:10.1785/0120090307.

Hardebeck, J.L., 2012. Seismicity of the Shoreline and Hosgri Faults, Estero Bay and Irish Hills, PowerPoint presentation at DCP.P SSHAC Workshop #2, 6 November.

Hardebeck, J.L., 2013. Geometry and earthquake potential of the Shoreline Fault, Central California, *Bulletin of the Seismological Society of America* **103** (1): 447–462.

Harland, W.B., 1971. Tectonic transpression in Caledonia Spitzbergen, *Geological Magazine* **108**: 27–42.

Howell, D.G., Crouch, J.K., Greene, H.G., McCulloch, D.S., and Vedder, J.G., 1980. Basin development along the late Mesozoic and Cenozoic California margin: A plate tectonic margin of subduction, oblique subduction and transform tectonics: in Ballance, P.F., and Reading, H.G. (editors), *Sediment in Oblique-Slip Mobile Zones*, International Association of Sedimentologists Special Publication, chap. 4, pp. 43–62.

Kingma, J.T., 1958. Possible origin of piercement structures, local unconformities, and secondary basins in the Eastern Geosyncline, New Zealand: *New Zealand Journal of Geology and Geophysics* **1**: 269–274.

Langenheim, V.E., 2014. Gravity, Aeromagnetic and Rock-Property Data of the Central California Coast Ranges, *U.S. Geological Survey Open-File Report 2013-1282*, 12 pp., <http://dx.doi.org/10.3133/ofr20131282>.

Lekkerkerk, H-J., van der Velden, R., Roders, J., Haycock, T., de Vries, R., Jansen, P., and Beemster, C., 2006. *Handbook of Offshore Surveying, Book Two*, Clarkson Research Services Limited, St Magnus House, London, 194 pp.

Lettis, W.R., Hanson, K.L., Unruh, J.R., McLaren, M., and Savage, W.U., 2004. Quaternary tectonic setting of south-central coastal California: in Keller, M.A. (editor), *Evolution of Sedimentary Basins/Offshore Oil and Gas Investigations—Santa Maria Province*, U.S. Geological Survey Bulletin 1995-AA, 24 pp.

Luyendyk, B.P., 1991. A model for Neogene crustal rotations, transtension, and transpression in Southern California, *Geological Society of America Bulletin* **103**: 1528–1536.

Mann, P., 2007. Global catalogue, classification and tectonic origins of restraining- and releasing bends on active strike-slip fault systems: in Cunningham, W.D., and Mann, P. (editors), *Tectonics of Strike-Slip Restraining and Releasing Bends*, Geological Society, London, Special Publications, vol. 290, pp. 13–142.

McClay, K., and Bonora, M., 2001. Analog models of restraining stepovers in strike-slip fault systems, *American Association of Petroleum Geologists Bulletin* **85** (2): 233–260.

Mitra, S., and Paul, D., 2011. Structural geometry and evolution of releasing and restraining bends: Insights from laser-scanned experimental models, *American Association of Petroleum Geologists Bulletin* **95** (7): 1147–1180.

NCS SubSea, Inc., 2011. Navigation Final Report, Diablo Canyon Power Plant 3D Geophysical Survey, Job Number J00344-FR-001-001, 18 pp.

Pacific Gas and Electric Company (PG&E), 1988. *Final Report of the Diablo Canyon Long Term Seismic Program*, U.S. Nuclear Regulatory Commission Enclosure 1, PG&E letter DCL-05-002, Docket No. 50-275 and No. 50-323.

Pacific Gas and Electric Company (PG&E), 2008. E-mail to Alan Wang and Vincent Gaddy (NRC) from Bill Guldmond (PG&E), Subject: Preliminary data for seismic discussion, with attachment, DCP.P\_Nov 20-2008\_v2 (3). ppt.

Pacific Gas and Electric Company (PG&E), 2011a. *Progress Report on the Analysis of the Shoreline Fault Zone, Central Coastal California*, Report to the U.S. Nuclear Regulatory Commission, PG&E Letter DCL-10-003, 36 pp.

Pacific Gas and Electric Company (PG&E), 2011b. *Report on the Analysis of the Shoreline Fault Zone, Central Coastal California*, Report to the U.S. Nuclear Regulatory Commission, January; available at [www.pge.com/myhome/edusafety/systemworks/dcpp/shorelinereport/](http://www.pge.com/myhome/edusafety/systemworks/dcpp/shorelinereport/).

Pacific Gas and Electric Company (PG&E), in preparation (2014). *The Central Coastal California Seismic Imaging Project Report*, August 2014.

Quennell, A.M., 1958. The structural and geomorphic evolution of the Dead Sea Rift, *Quarterly Journal of the Geological Society of London* **114**: 1–14.

Reading, H.G., 1980. Characteristics and recognition of strike-slip fault systems: in Ballance, P.F., and Reading, H.G. (editors), *Sediment in Oblique-Slip Mobile Zones*, International Association of Sedimentologists Special Publication, chap. 4, pp. 7–26.

Rodgers, D.A., 1980. Analysis of pull-apart basin development produced by en echelon strike slip faults: in Ballance, P.F., and Reading, H.G. (editors), *Sediment in Oblique-Slip Mobile Zones*, International Association of Sedimentologists Special Publication chap. 4, pp. 27–41.

Sheriff, R.E., 1982. *Structural Interpretation of Seismic Data*, American Association of Petroleum Geologists, 73 pp., ISBN 0-89181-172-9.

Sheriff, R.E., and Geldart, L.P., 1995. *Exploration Seismology*, Cambridge University Press, Second Edition.

Sliter, R.W., Triezenberg, P.J., Hart, P.E., Watt, J.T., Johnson, S.Y., and Scheirer, D.S., 2009. *High-Resolution Seismic Reflection and Marine Magnetic Data Along the Hosgri Fault Zone, Central California*, U.S. Geological Survey Open-File Report 2009-1100; <http://pubs.usgs.gov/of/2009/1100>.

Tchalenko, J.S., 1970. Similarities between shear zones of different magnitudes, *Geological Society of America Bulletin* **81**: 1625-1640.

Wilcox, R.E., Harding, T.P., and Seely, D.R., 1973. Basic wrench tectonics, *American Association of Petroleum Geologists Bulletin* **57**: 74-96.

Willingham, C.R., Rietman, J.D., Heck, R.G., and Lettis, W.R., 2013. Characterization of the Hosgri Fault Zone and adjacent structures: in Keller, M.A. (editor), *The Offshore Santa Maria Basin, South-Central California*, U.S. Geological Survey Bulletin 1995-CC, Evolution of Sedimentary Basins/Onshore Oil and Gas Investigations, Santa Maria Province.

Yilmaz, O., 2001. *Seismic Data Analysis, Processing, Inversion, and Interpretation of Seismic Data*, Society of Exploration Geophysicists, Investigations in Geophysics No. 10, 2nd Ed., Tulsa, OK, 2 volumes, 2027 pp

## INDEPENDENT VERIFICATION OF REPORT

Attachment 1

## REPORT VERIFICATION SUMMARY

Item	Parameter	Yes	No*	N/A*
1	Purpose is clearly stated and the report satisfies the Purpose.	X		
2	Data to be interpreted and/or analyzed are included or referenced.	X		
3	Methodology is appropriate and properly applied.	X		
4	Assumptions are reasonable, adequately described, and based upon sound geotechnical principles and practices.	X		
5	Software is identified and properly applied. Validation is referenced or included, and is acceptable. Input files are correct.	X		
6	Interpretation and/or Analysis is complete, accurate, and leads logically to Results and Conclusions.	X		
7	Results and Conclusions are accurate, acceptable, and reasonable compared to the Data, interpretation and/or analysis, and Assumptions.	X		
8	The Limitation on the use of the Results has been addressed and is accurate and complete.	X		
9	The Impact Evaluation has been included and is accurate and complete.	X		
10	References are valid for intended use.	X		
11	Appendices are complete, accurate, and support text.			X

\* Explain "No" or "N/A" entries. (For example, Items 3 thru 7 would be N/A for a data report that simply presents the collected data.)

Comments (use additional pages as necessary):

Comment 1: I was also one of the two ITRs for Rev. 0 of this report. This ITR of Rev. 1 concentrated on the changes to the report and figures listed in the Record of Revisions on page 2 of this report. This ITR also included review of the text and figure edits provided by the PG&E Technical Editor. My comments have been discussed with the authors and subsequently resolved.

Comment 2: The appendix was prepared by Fugro Consulting, Inc. (FCL) and subject to FCLs internal QA process and not separately reviewed in this ITR.

Verifier (ITR):

Jan D. Rietman  
(name/signature)

9/4/2014  
(date)